The role of the intraspecific variability of hydraulic traits for modelling the plant water use in different European forest ecosystems

C.D. Jiménez-Rodríguez[1], M. Sulis[1], and S. Schymanski[1]

[1]Environmental Research and Innovation (ERIN) Department, Luxembourg Institute of Science and Technology (LIST), Belvaux, 4422, Luxembourg.

Corresponding author: César Jiménez-Rodríguez (cesar.jimenez@list.lu, cdjimenezcr@gmail.com)

Key Points:

- We explore the impact of the intraspecific variability of plant hydraulic traits on the simulated transpiration by CLM5.

- We find that a choice of plant hydraulic traits that reproduces observed plant transpiration also reduces simulated water stress.

- We demonstrate the critical role of the maximum xylem conductance in the model and its dependency on factors other than vegetation type.

Abstract

The drought resilience of forest ecosystems is generally believed to strongly depend on the dominant tree species' hydraulic traits. These traits define the maximum water transport capacity and the degree of vulnerability to hydraulic failure of a given tree species. This work evaluates the effect of the intraspecific variability of hydraulic traits on the simulated tree water use in the Community Land Model (CLM, version 5.0). We selected two broadleaved tree species with contrasting phenologies, geographical distribution, degrees of vulnerability to hydraulic failure, and water use strategies. We performed a series of numerical experiments by modifying the parameters of the plant vulnerability curve and the maximum xylem hydraulic conductance to account for the variability within each tree species. Our prescribed parameter sets represent vulnerable and resistant tree responses to the water deficit. At sites with an ample water supply, the resistant configuration simulates reduced water stress and increased transpiration compared to the vulnerable configuration, whereas at temporarily dry sites, the model results are counter-intuitive when water availability is the limiting factor. The numerical experiments demonstrate the emergent role of the maximum xylem conductance as a modulator of the plant water use strategy and the simulated transpiration. Using the default value for maximum xylem conductance, the model tends to overestimate the spring transpiration at drier sites, forcing the vegetation to experience unrealistic water stress in summer. Our findings suggest that the parameterization of maximum xylem conductance is an important and yet unresolved problem in the CLM and similar land surface models.

Plain Language Summary

The survival of trees under drought conditions depends on their adaptation to water scarcity. Part of this adaptation is characterized by specific plant traits, which are an important component of the Land Surface Models, largely determining the relationship between soil moisture and canopy gas exchange. Our study explores how the variability of specific plant traits of individual tree species may affect the model's ability to reproduce the observed water use by forest stands in Europe. In climates with a pronounced summer dry period, we found that the default model settings overestimate the vegetation water use in the early growing season, when water is abundant, resulting in severe water stress and underestimation of transpiration as the dry season progresses. Specifically, we demonstrate that the rarely considered plant trait representing the maximum water transport capacity plays an essential role in controlling the magnitude of simulated water use and that adjustments to this parameter greatly help to reproduce observed vegetation water use in seasonally dry climates.

1 Introduction

The recent worldwide increase in drought incidence and severity (He et al., 2020) has been associated with high rates of tree mortality (Powers et al., 2020; Senf et al., 2020), altered soil carbon and nitrogen dynamics (Deng et al., 2021), and a diminution in forest evaporation (Lansu et al., 2020; Lindroth et al., 2020). The severity of drought impacts on forest ecosystems and the spatial extent of them depends on the difference between precipitation and potential evaporation, atmospheric water demand, and forest resilience. The latter reflects the lumped vulnerability of individual trees (Haberstroh & Werner, 2022) and is driven by the safety

59 mechanisms used to overcome disturbances in the whole tree hydraulic system (Arend et al.,
60 2022).

61   The resilience of a species to water stress is commonly expressed in the plant
62 vulnerability curve and the recovery patterns shown by the tree species (Klein et al., 2018). This
63 curve postulates a continuous decline of plant organ conductance with declining water pressure
64 in the plant organ (Sperry & Love, 2015; Venturas et al., 2017). The parameters of the curve
65 differ among and within tree species (Rosner et al., 2019), and are influenced by the provenance
66 of the species (Hajek et al., 2016; Lobo et al., 2018) and xylem features such as lignin content
67 (Pereira et al., 2018). This relationship between hydraulic conductivity and pressure has been
68 analyzed across species and biomes (Choat et al., 2012), allowing to quantify the degree of
69 vulnerability to hydraulic failure (Venturas et al., 2017). Vulnerable trees commonly have an
70 early loss of conductance, small safety margins, and low wood density. Resistant trees have
71 vulnerability curves ranging from gradual to steep responses at lower water potentials. These
72 trees commonly have large safety margins and high wood density (Meinzer & McCulloh, 2013;
73 Mrad et al., 2019). The degree of vulnerability to hydraulic failure is related to the trade-off
74 between xylem safety and efficiency (Gleason et al., 2016; Hacke et al., 2006; Venturas et al.,
75 2017). This trade-off requires the coordination of the plant hydraulic traits and water use strategy
76 (WUS), which ranges from aggressive to conservative (Flo et al., 2021; Mrad et al., 2019). Also,
77 the WUS is influenced by the stomatal regulation capacity of the tree species (Konings &
78 Gentine, 2017) and modulated by the vapor pressure deficit irrespective of the soil water content
79 (Fu et al., 2022; Novick et al., 2019).

80   The plant hydraulic theory is numerically implemented in models using either a plant
81 pipe model, a porous media model, or an electrical analogy model (see Mencuccini et al. (2019)
82 for a more detailed overview). Plant pipe models follow the Hagen-Poiseulle law and require the
83 use of allometric scaling laws (Li et al., 2021; Mrad et al., 2018), whereas porous media models
84 are based on Richards equation assuming that water movement through the xylem mimics an
85 unsaturated porous media flow (Christoffersen et al., 2016; Li et al., 2021). Finally, the electrical
86 analogy models resemble an electrical circuit with resistance and capacitance parameters that
87 control the water flow following Darcy's law (Eller et al., 2018; Li et al., 2021). An electrical
88 analogy model has low to moderate computational requirements making it a suitable model for
89 implementation in large scale Land Surface Models (LSMs). For example, the Community Land
90 Model 5.0 (CLM5, Lawrence et al., 2019) implements an electrical analogy model using the
91 plant vulnerability curve to downscale the segment conductance according to the percent loss of
92 conductance (PLC) (Kennedy et al., 2019). Given its recent implementation, the simulated plant
93 hydraulic response (e.g., vulnerability to hydraulic failure) of CLM5 during drought conditions
94 and across different forested ecosystems has not yet been evaluated in detail. Specifically, it has
95 never been examined in detail to what extent the current (and default) plant hydraulic
96 formulation and parameterization of the model reproduces realistic transpiration rates and plant
97 water status under varying soil moisture availability and atmospheric water demand.

98   The implementation of the plant hydraulic formulation in LSMs relies on the definition of
99 plant hydraulic traits within the Plant Functional Type (PFT) classification framework (Bonan et
100 al., 2002). This classification assumes that hydraulic traits are spatially homogeneous and
101 temporally fixed within predefined vegetation categories, which is equivalent to assuming the
102 same drought sensitivity within the same PFT class. Several studies have addressed the
103 implications associated with the loss of diversity in the PFT classification in terms of water and

104 carbon dynamics by using deterministic or stochastic coordinated plant attributes (Christoffersen
105 et al., 2016; Pappas et al., 2016; Wang et al., 2012; Xu et al., 2016) or by exploiting plant trait-
106 climate relationships (Verheijen et al., 2013). A recent study by Butler et al. (2022) showed that
107 the aggregation of allocation and hydraulic traits into PFTs reduces the productivity of the
108 modelled ecosystem with respect to the flux data of sites with a strong dependency on vegetation
109 phenology. Overall, representing the plant trait inter- and intraspecific diversity within the PFT
110 broad classification scheme remains a challenging task requiring the characterization of the
111 emergent plant response by coordinating water use strategies with the xylem vulnerability
112 (Skelton et al., 2015). While the trade-off between plant hydraulic traits has been addressed in
113 previous studies using detailed plant hydrodynamic models (e.g., Mirfenderesgi et al. (2019)),
114 the coordination between hydraulic traits and water use strategies remains unexplored for the
115 plant hydraulic framework implemented in LSMs. Addressing this issue may provide an
116 opportunity to define optimal strategies for large-scale parameterizations of key plant hydraulic
117 traits (e.g., maximum xylem conductance), which are rarely documented in existing hydraulic
118 trait databases.

119   This manuscript aims to evaluate the effect of the intraspecific variability of plant
120 hydraulic traits on the simulated transpiration response of two contrasting tree species in CLM5.
121 The intraspecific variability of plant hydraulic traits defines the spectrum of vulnerability
122 responses to hydraulic failure and the water use strategies of each species. This spectrum
123 considers that individual tree species have different boundaries determining their degree of
124 vulnerability to hydraulic failure. Our hypothesis is that vulnerable trees transpire more than
125 resistant trees under unstressed water conditions and perform poorly during dry periods. On the
126 other hand, resistant trees maintain low transpiration rates but experience less stress on the plant
127 hydraulic system. For each species, we distinguish between a resistant and vulnerable hydraulic
128 trait configuration by extracting from the reported parameter sets for that species the plant
129 vulnerability curve with the minimum and maximum loss of 50% of conductance (Ψ_{p50}) value,
130 respectively. This hypothesis is evaluated for two broadleaved tree species, *Quercus ilex* L. and
131 *Fagus sylvatic*a L., with contrasting phenologies and provenances. The results of point-scale
132 numerical experiments with CLM5 based on each parameterization are compared to the sap flux
133 observed at four experimental sites across Europe. The representation of the simulated
134 vulnerability to hydraulic failure and the water use strategy of each species are interpreted using
135 the simulated leaf water stress factor (β) and percent loss of conductance (PLC) in different plant
136 organs.

2 Materials and Methods

2.1 Tree Species and Experimental Sites

139   The tree species selected for this study, *Fagus sylvatica* L. and *Quercus ilex* L., belong to
140 the same botanical family (Fagaceae) but differ in their phenology and spatial distribution in
141 Europe (Figure 1). *Fagus sylvatica* is a deciduous broadleaved tree distributed in Central and
142 Western Europe, from Southern Italy to Southern Norway. This tree species grows from sea level
143 to 1000 m a.s.l., with a higher upper elevation limit in dryer regions. It does not survive in
144 locations with poor drainage or stagnant water, and its relatively shallow root system makes it
145 susceptible to drought and high temperatures (Houston Durrant et al., 2016; von Wuehlisch,
146 2008). *Quercus ilex* is a broadleaved evergreen species that grows as a tree or shrub. It inhabits
147 the Mediterranean basin from the coast up to 1800 m a.s.l., can survive low temperatures, and its

148 sclerophyllous character allows transpiration to be reduced during dry periods and its resistance
149 to drought to be improved (de Rigo & Caudullo, 2016; Schirone et al., 2019).

150   Two experimental sites for each species were selected from the SAPFLUXNET database
151 (Poyatos et al., 2020). *Fagus sylvatica* is the dominant tree species in Hesse (France, FR-Hes)
152 and Hinnensee (Germany, DE-Hin), over the sampling periods of 2001-2005 and 2012-2014,
153 respectively (Table 1). Both sites have a temperate oceanic climate (Cfb) according to Köppen-
154 Geiger's climate classification (Beck et al., 2018), with no significant intraseasonal precipitation
155 variability. The stand age marks the main difference between these two sites; trees in FR-Hes
156 were 34 years old during the selected measurement period while those in DE-Hin were more
157 than 200 years old. The mean tree diameter reflects this age difference, with 12.9 cm at FR-Hes
158 and 43.6 cm at DE-Hin. *Quercus ilex* is the dominant tree species in Puechabon (France, FR-
159 Pue) and Alto Tajo (Spain, ES-Alt). These sites cover the monitoring periods 2001-2005 and
160 2012-2014, respectively. The climate differs slightly between these two sites; FR-Pue has a hot-
161 summer Mediterranean climate (Csa) while ES-Alt has a warm-summer Mediterranean climate
162 (Csb). The different elevations of the sites explain the differences in climate classification (Table
163 1). Despite a lack of differences in the stand age between these two sites, the diameter recorded
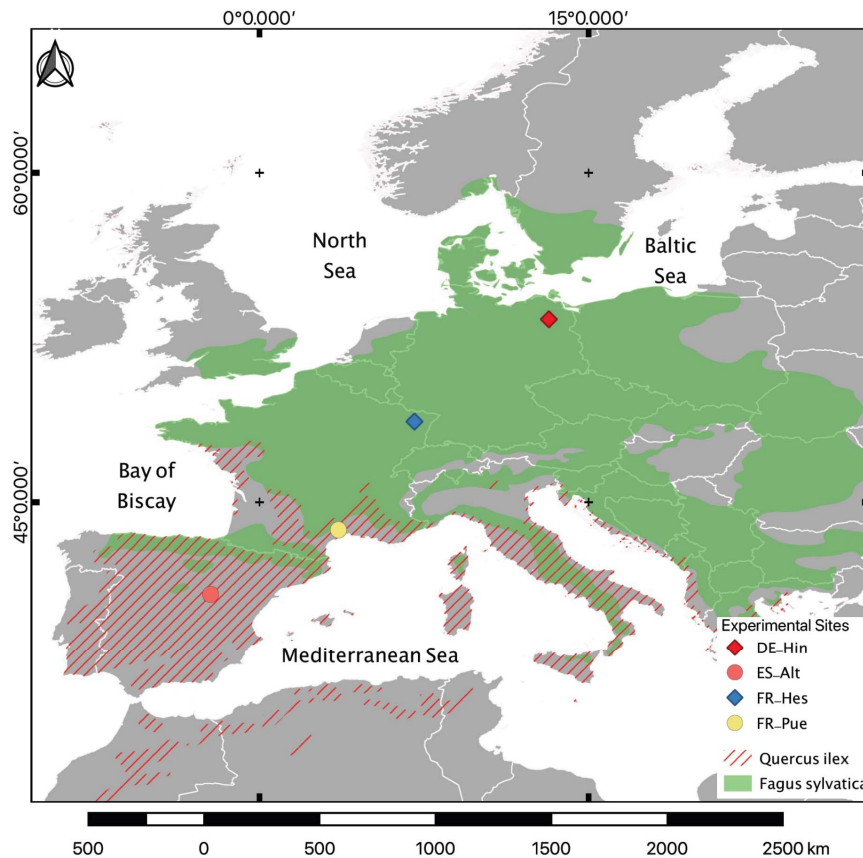164 for the trees in FR-Pue (9.1 cm) is much smaller than the diameter in ES-Alt (24.4 cm).

165

166 **Figure 1**. Geographical location of the four experimental sites and the spatial distribution of
167 *Fagus sylvatica* L. and *Quercus ilex* L. across Europe. The spatial distribution of the tree species
168 is based on Mauri et al. (2022).

169 2.2 Model Setup

170 The Community Land Model version 5.0 (CLM5, Lawrence et al. (2019)) was
171 implemented at each experimental site using point-scale setups. Hourly atmospheric forcing was
172 retrieved from the SAPFLUXNET dataset. This dataset includes precipitation, wind speed, air
173 temperature, relative humidity, and incoming shortwave radiation. The incoming longwave
174 radiation was calculated according to An et al. (2017) using the vapor pressure deficit and
175 temperature. The COSMO-REA6 reanalysis product (Bollmeyer et al., 2015) was used to fill in
176 the missing variables (i.e., atmospheric pressure) and temporal data gaps for each site. The
177 monthly leaf area index (LAI) in $m^2\ m^{-2}$ was determined based on the Global Land Surface
178 Satellite (GLASS) product (Liang et al., 2013, 2014) for the different periods under analysis. The
179 monthly stem area index (SAI) in $m^2\ m^{-2}$ was retrieved from the global surface dataset of the
180 model as described in (P. J. Lawrence & Chase (2010). The root area index (RAI) in $m^2 m^{-2}$ is
181 calculated in the model (see Equation 2.11.15 of the technical documentation (UCAR, 2020))
182 based on plant functional type-specific parameters such as the LAI, SAI, root fraction in each
183 soil layer, and the root-to-shoot ratio. The main soil characteristics (e.g., soil texture, organic
184 matter content) were taken from Bonan et al. (2002), while the depth to bedrock was taken from
185 Pelletier et al. (2016). Multi-year spin-up runs were performed for each experimental site by
186 reinitializing soil moisture and soil temperature until a dynamic equilibrium condition was
187 reached. The tree species at the selected sites pertain to two distinctive plant functional types
188 (PFTs), with *Fagus sylvatica* representing the Temperate Broadleaf Deciduous Tree (BDT) in
189 FR-Hes and DE-Hin and *Quercus ilex* representing the Temperate Broadleaf Evergreen Tree
190 (BET) in FR-Pue and ES-Alt; see Table 2 for the default plant hydraulic configuration (DC) of
191 these two PFTs.

192 2.3 Plant Vulnerability Curve

193 The plant vulnerability curve (PVC) implemented in CLM5 (Equation 1) determines the
194 plant segment specific hydraulic conductance k ($mm_{H2O}\ mm_{H2O}^{-1}s^{-1}$) based on three parameters:
195 the xylem pressure inducing 50% loss of hydraulic conductance (Ψ_{p50}, MPa), the non-
196 dimensional sigmoidal shape parameter of the curve (c_k), and the maximum plant hydraulic
197 conductance (k_{max}, $mm_{H2O}\ mm_{H2O}^{-1}s^{-1}$). CLM5 uses k_{max}, Ψ_{p50} and c_k as static parameters
198 that may differ between plant segments (i.e., root, xylem, and sunlit and shaded leaf) and PFTs.
199 The plant hydraulic system of CLM5 uses k to determine the flux per plant segment by applying
200 a Darcy's law equation, where the reference area varies between plant segments: the leaf area
201 index (LAI, m^2m^{-2}) for the stem-to-leaf, the stem area index (SAI, m^2m^{-2}) for the root-to-stem,
202 and the root area index (RAI, m^2m^{-2}) for the soil-to-root segment. A detailed description of the
203 equations used by the plant hydraulic system of CLM5 is provided in Kennedy et al. (2019) and
204 Lawrence et al. (2019).

205

$$k = k_{max}2^{-\left(\frac{\Psi}{\Psi_{p50}}\right)^{c_k}}$$	Equation 1

206   2.4. Intraspecific Variability of Plant Hydraulic Traits

207 The intraspecific variability of both tree species was determined based on the loss of hydraulic
208 conductance at 12%, 50%, 88%, and in some cases at 10% (Ψ_{p12}, Ψ_{p50}, Ψ_{p88}, and Ψ_{p10},
209 respectively), as reported in the Xylem Functional Traits (XFT) database (Choat et al., 2012).
210 Additional data sources for *Fagus sylvatica* were retrieved from the literature review; see table
211 S1 for a complete list of references for the additional data. The c_k parameter of each dataset was
212 determined by converting the reported slope of the vulnerability curve at Ψ_{p50} to c_k or by solving
213 the CLM vulnerability curve for c_k and inserting any provided combination of PLC and Ψ_{p10}, or
214 Ψ_{p12}, or Ψ_{p88} values reported in the XFT database, with a preference for Ψ_{p10} or Ψ_{p12} if available.
215 The procedure to determine the c_k parameter assumes that Equation 1 follows the Weibull
216 distribution, allowing to use the vulnerability curve formulation from Domec and Gartner (2001).
217 From this formulation, we derived Equation 2 to calculate the c_k parameter based on the Ψ_{p50}, the
218 slope of the curve (s) at Ψ_{p50} (Pa^{-1}), and V as a constant dimensionless value of 34.66. To
219 determine V, we deduced Equation 3 from Domec and Gartner (2001) and inserted the percent
220 loss of conductivity (τ_{50}) of 50%. Equation 4 is used to calculate s (Pa^{-1}) using the slope at any
221 specific loss of conductivity (τ). This indicator is calculated with Equation 5 using τ in %, Ψ_{p50},
222 and Ψ_x that represents the matric potential at the selected τ. Finally, the two curves with the
223 highest and lowest Ψ_{p50} values were selected for each species to represent the vulnerable (VC)
224 and resistant (RC) response, respectively (Figure 2); see Table 2 for more details on the obtained
225 values.

226

| $$c_k = \frac{\Psi_{p50} \cdot s}{V}$$ | Equation 2 |

227

| $$V = (\tau_{50} - 100) \cdot \ln\left(1 - \frac{\tau_{50}}{100}\right)$$ | Equation 3 |

228

| $$s = -25 \frac{\log\left(\frac{100 - \tau}{\tau}\right)}{\Psi_x - \Psi_{p50}}$$ | Equation 4 |

229

230   The xylem water potentials of *Fagus sylvatica* have a narrow distribution, with the Ψ_{p12},
231 Ψ_{p50}, and Ψ_{p88} values ranging from -2.0 MPa to -5.0 MPa (Figure 2). The two extreme curves
232 obtained from this dataset have a steep decline of hydraulic conductance with the diminution of
233 water potentials, with a small range in c_k (1.73 to 3.33) and Ψ_{p50} (-1.9 MPa to -4.7 MPa) values
234 (Table 2). *Quercus ilex* has a larger range of xylem water potentials than *Fagus sylvatica*,
235 ranging from -0.5 MPa to -7.0 MPa. This species shows a large difference between the extreme
236 vulnerability curves, with c_k values ranging from 1.70 to 8.04 MPa and Ψ_{p50} from -1.23 to -5.72
237 MPa for the VC and RC, respectively.

238   The k_{max} values used by default in CLM5 are assumed constant for the different PFTs and
239 homogeneous across the different plant organs (i.e., root, xylem, and leaf). k_{max} values for each
240 plant segment can be determined based on the experimental specific hydraulic conductance (k_s,

241   kg m^{-2}MPa^{-1}s^{-1}), which is defined as the flow rate per cross sectional area per unit of pressure
242   difference along a plant segment (kg m^{-2}MPa^{-1}s^{-1}) (Eamus et al., 2016). However, a standard
243   procedure for determining k_{max} for its use in CLM5 (i.e., at PFT level and for each plant segment)
244   from tree- and plant organ-specific information existing in literature has not been specified yet.
245   Therefore, considering the large uncertainty in estimating this parameter and the unknown effect
246   of its variability, we arbitrary choose a range of values between one order of magnitude above
247   (2.0 x 10^{-7} mm$_{H2O}$ mm$_{H2O}$$^{-1}$s^{-1}) and below (2.0 x 10^{-9} mm$_{H2O}$ mm$_{H2O}$$^{-1}$s^{-1}) the default value (2.0 x
248   10^{-8} mm$_{H2O}$ mm$_{H2O}$$^{-1}$s^{-1}) of the model. The upper and lower values of this variability range are
249   referred to from now as high (Hk_{max}) and low (Lk_{max}) xylem conductance, respectively.
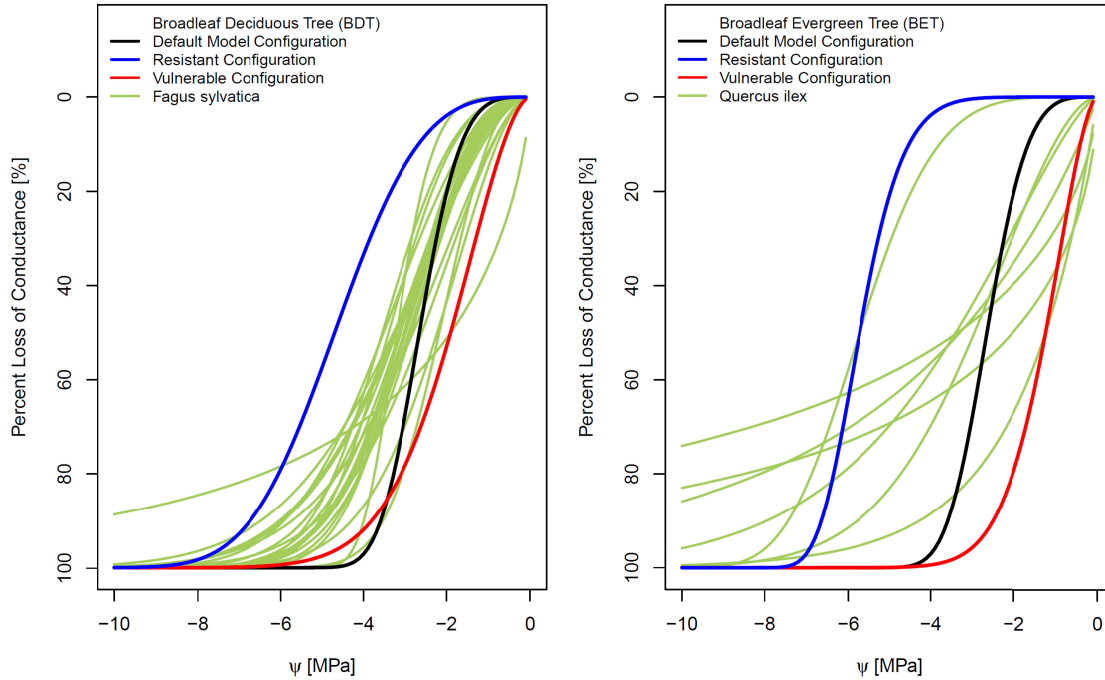

250

Figure 2. Spectrum of the vulnerability curves of *Fagus sylvatica* L. (left plot) and *Quercus ilex*
L. (right plot). The solid blue, red, and black lines represent the resistant, vulnerable, and default
vulnerability curves used in the numerical experiments, respectively. The solid green lines show
the full set of vulnerability curves for each species.

255

2.5. Numerical Experiments

257   The role of the intraspecific variability of plant hydraulic traits in contrasting tree species
258   was examined based on a series of numerical experiments. These experiments aimed to assess to
259   what extent the plant hydraulics representation of CLM5 reproduces the measured transpiration
260   of each experimental site based on the spectrum of vulnerability to the hydraulic failure of each
261   tree species (Table 2).

262   The first set of experiments compared the effect of the PVC shape on the distribution of
263   PLC values, leaf water stress (β), and the transpiration simulated by the model. The PVC shape
264   parameters determine the steepness of the hydraulic response (c_k) and the range of water
265   potentials at which the plant will start experiencing extreme water stress (Ψ_{p50}). We hypothesized

266   that the RC describes a plant response less affected by low soil water potentials, while the VC
267   describes a plant response with a high susceptibility to hydraulic failure at low water potentials.

268   The second set of experiments explored the role of k_{max} in constraining the whole plant
269   water use strategy of the different tree species. This was achieved by changing the k_{max} value to
270   the high (Hk_{max}) and low (Lk_{max}) xylem conductance while keeping the default model
271   configuration for the shape parameters (Table 2). Finally, two additional intermediate values
272   were added to this experiment representing a half order of magnitude difference between the
273   boundaries and the default k_{max} (1.1 x 10^{-7} mm_{H2O} $mm_{H2O}^{-1}s^{-1}$ and 1.1 x 10^{-8} mm_{H2O} $mm_{H2O}^{-1}s^{-1}$)
274   and are referred to as intermediate-high (IHk_{max}) and intermediate-low (ILk_{max}) xylem
275   conductance, respectively.

276   The third set of experiments aimed to evaluate the role of coordinated changes in safety
277   (i.e., shape parameters) and transport capacity (i.e., maximum xylem conductance). We analyzed
278   the plant hydraulic response simulated by CLM5 using the best fitted k_{max} value obtained for
279   each site in the second set of experiments together with both Ψ_{p50} and c_k values used in the first
280   set of experiments (Table 2). That is, the response of each vulnerable and resistant model
281   configuration was evaluated across a wide spectrum of xylem conductance. We hypothesized
282   that a resistant tree species (i.e., with low Ψ_{p50}) associated with high k_{max} values would
283   experience more stress (i.e., large degree of vulnerability) than a vulnerable tree species having a
284   low k_{max}.

285   2.6. Data Analysis

286   2.6.1. Reference Evaporation

287   Equation 5 is based on Equation 6 from Allen et al. (1998), and calculates the reference
288   evaporation (E_o) used as a descriptive variable of the atmospheric water demand for each
289   experimental site. Equation 5 assumed a reference crop of 0.12 m height, a surface resistance of
290   70 s m^{-1}, and an albedo of 0.23. This equation requires wind speed (u) in m s^{-1}, net radiation (R_n)
291   and ground heat flux (G) both in MJ $m^{-2}d^{-1}$, air temperature (T) in C, and the actual and saturated
292   vapor pressures (e_a and e_s, respectively) in kPa. G was extracted from the modeled results of the
293   default configuration of each experimental site. The slope of the saturation vapor pressure curve
294   at air temperature (Δ, kPa K^{-1}) was computed using Equation 6, based on Equation 13 from Allen
295   et al. (1998). The psychrometric constant (γ) was estimated with Equation 7 based on Equation 8
296   from Allen et al. (1998), where λ is the latent heat of vaporization (2.45 MJ kg^{-1}), c_p is the
297   specific heat at constant pressure (1.013 x 10^{-3} MJ kg^{-1} K^{-1}), p is the atmospheric pressure (kPa),
298   and ϵ is the molecular weight ratio of water vapor and dry air (0.622).

299

$$E_o = \frac{0.408 \cdot \Delta \cdot (R_n - G) + \gamma \frac{900}{T + 273} \cdot u \cdot (e_s - e_a)}{\Delta + \gamma \cdot (1 + 0.34 \cdot u)}$$	Equation 5

300

$$\Delta = \frac{4098 \cdot \left(0.6108 \cdot exp^{\left(\frac{17.27 \cdot T}{T + 273.3}\right)}\right)}{(T + 237.3)^2}$$	Equation 6

301

$$\gamma = \frac{c_p p}{\epsilon \lambda}$$

Equation 7

2.6.2. Upscaled Transpiration

Observed forest transpiration (E_T) in mm hr^{-1} was calculated based on the hourly and sub-hourly sap flux of individual trees (Q_{tree}) in cm^3 hr^{-1} available on the SAPFLUXNET data set (Poyatos et al., 2020). We used equation 8 to obtain E_T and summarized it in daily time steps following the recommendations of Nelson et al. (2020). Equation 8 requires Q_{tree} aggregated in hourly fluxes per tree (m^3 hr^{-1}tree^{-1}), the basal tree area (Ω_{tree}) in m^2 tree^{-1}, the stand basal area (Ω_{stand}) in m^2 m^{-2}, and the number of measured trees (n). All the information required in Equation 8 is available on the SAPFLUXNET data set for each site. The stand basal area of DE-Hin was missing in the SAPFLUXNET data set, so we obtained it from Moreno et al. (2017) according to the geographical location of the plot.

312

$$E_T = \frac{\Omega_{stand}}{n \cdot 10^3} \cdot \sum_{tree=1}^{n} \frac{Q_{tree}}{\Omega_{tree}}$$

Equation 8

2.6.3 Plant Water Stress

The plant water stress was evaluated by comparing the percent loss of conductance (PLC) and the transpiration water stress parameter (β). The PLC was calculated using Equation 9 at the root-stem (hereafter named stem) and stem-leaf (hereafter named leaf) plant segments. This equation uses the simulated (k) and the maximum (k_{max}) plant organ conductance. The water stress parameter β was calculated as a weighted average of shade and sunlit components according to their corresponding LAI components. Further details on the mathematical formulation of the water stress factor of CLM5 are provided in Kennedy et al. (2019).

321

$$PLC = 100 \cdot \left(1 - \frac{k}{k_{max}}\right)$$

Equation 9

3. Results

The impact of the different plant hydraulic parametrizations was investigated by comparing the simulated time series of transpiration (E_{Tm}) to the upscaled sap flux measurements (E_T). The comparison was carried out for the spring, summer, and autumn seasons. Furthermore, a comprehensive insight into the simulated plant hydraulic response was gained by analyzing the temporal evolution and probability density of PLC, the transpiration water stress parameter (β), and the water potentials across the soil-vegetation continuum (Ψ).

3.1. Reference Evaporation and Measured Transpiration

Figure 3 shows the seasonal distribution of E_o and E_T for the four sites and two tree species selected. For most of the seasons, the atmospheric water demand is two- and four-times larger than the E_T in FR-Hes/DE-Hin and FR-Pue/ES-Alt, respectively. It is worth noticing that

despite belonging to the same climate classification, the DE-Hin and FR-Hes sites have highly
contrastingly E_o values. This difference is explained by a lower mean annual precipitation (606.4
mm yr^{-1}) and temperature (8.7 °C) at DE-Hin compared to FR-Hes, which receives 1003.8 mm
yr^{-1} of precipitation and experiences a mean annual temperature of 9.97 °C. Seasonal E_T patterns
differ strongly among species and seasons, with sites dominated by *Fagus sylvatica* (i.e., FR-Hes
and DE-Hin) showing values close to 0 in spring and autumn due to the deciduousness of the
forest species. In contrast, the evergreen *Quercus ilex* at FR-Pue and ES-Alt express smaller
intraseasonal variations, with greater spring and autumn E_T, but smaller values in summer
compared to the *Fagus sylvatica* sites.

Figure 3. Seasonal variation of measured daily transpiration (E_T) and reference evaporation (E_o)
of the four forested sites in Europe. The area of the violin plots represents the data density
distribution. The horizontal line is the median of the data set with the respective value. The black
box represents the first and third quartiles of the data set. The elongated tales outwards from the
black boxes represent the data outliers.

3.2. Effects of Changing the Shape of the Vulnerability Curve

The experimental sites dominated by *Fagus sylvatica* have similar measured and modeled
transpiration values (Figure 4), with minor differences during the summer and autumn seasons,
but significant over-estimation of E_T in early spring. Note that for both deciduous sites, the sap

353   flow starts after the 105th day of the year, around the time of leaf flush, whereas the LAI values
354   used in our simulations also include the understory of the forest, and therefore likely over-
355   estimate early season tree LAI (see Figure S1). Figure 4 indicates that there are marginal
356   differences at both sites (i.e., FR-Hes and DE-Hin) when representing a vulnerable (VC) and
357   resistant (RC) shape of the vulnerability curve. As expected, the VC tends to produce, especially
358   during the summer period, lower transpiration rates and higher water stress conditions
359   represented by low β values. These stress conditions are mainly found at the stem-leaf level with
360   the median of the PLC values going beyond 12% while those at the root-stem level remain close
361   to zero. The comparison of the distribution of the PLC values at different plant levels (i.e., root-
362   stem and stem-leaf) with those of the β stress factor provides some additional insights into the
363   relative effect of stomata and plant hydraulics on the simulated transpiration response.

364   The effects of changing the shape of the vulnerability curve are remarkably different at
365   the evergreen sites (i.e., FR-Pue and ES-Alt) populated with *Quercus ilex* species (Figure 4). At
366   these sites, the default (DC) plant hydraulic model parameterization largely overestimates the
367   transpiration response during spring/early summer (see Figure S1), which leads to a strong
368   underestimation of E_T during prolonged dry conditions followed by a slow recovery in autumn.
369   Counterintuitively, this tendency is amplified by the resistant configuration (RC) and is
370   alleviated by the vulnerable configuration (VC) of plant hydraulics, with this latter simulating
371   higher transpiration rates during most of the summer. The unexpected model response is
372   confirmed by the distribution of the simulated water stress factor and PLC values, with the
373   response of the RC reflecting a higher level of hydraulic failure compared to DC and VC during
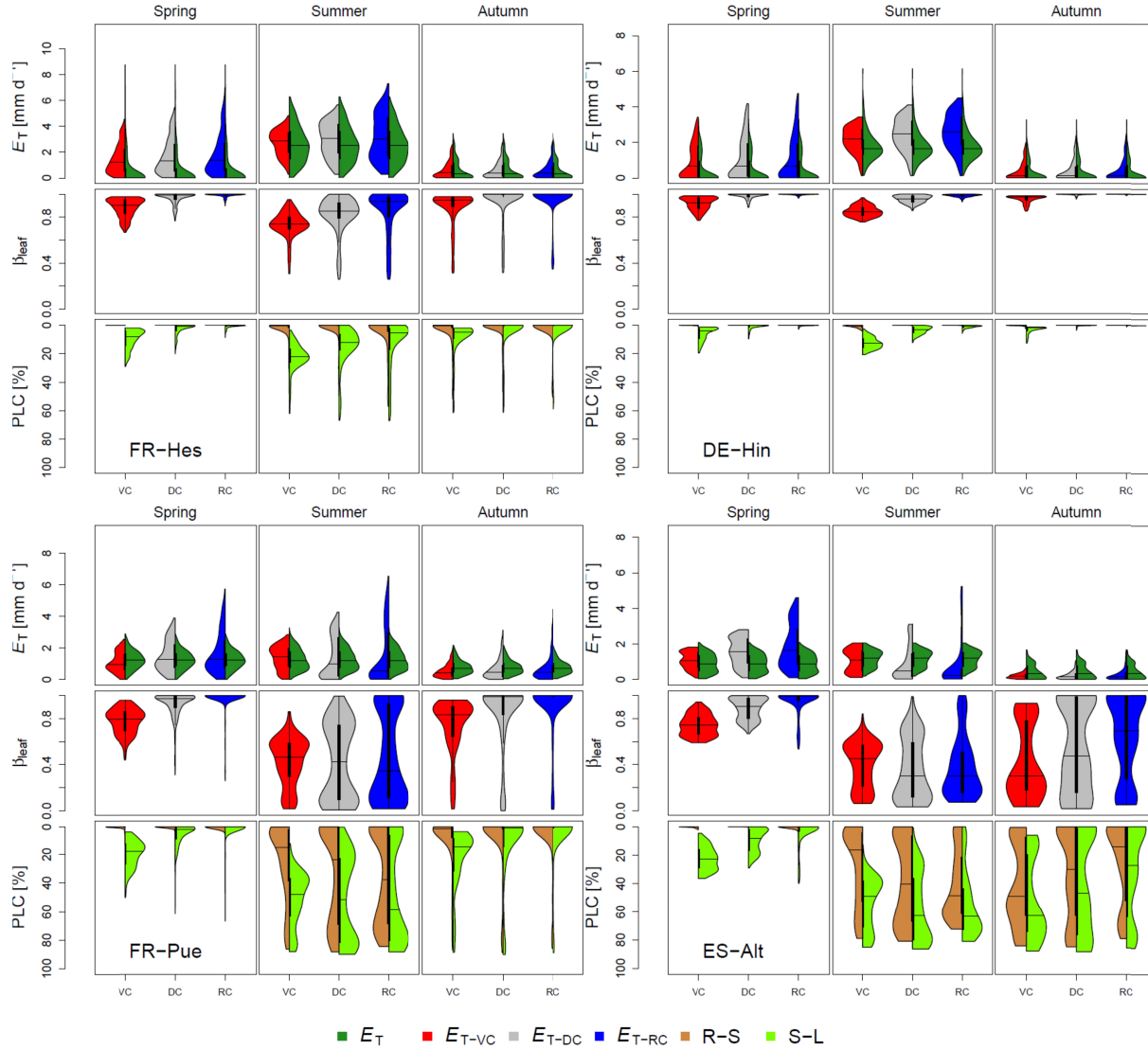374   the summer.

Figure 4. Seasonal distribution of daily transpiration (E_T), leaf water stress factor (β) and percent loss of conductance (PLC) for each experimental site showing the responses to changes in the shape parameters (i.e., Ψ_{p50} and c_k) of the plant vulnerability curve. Each violin plot contains the multiannual data for each site and season. The distribution of E_T is contained in the upper plot of each site (solid dark green). The vulnerable (VC), default (DC), and resistant (RC) configurations are represented by red, grey, and blue solid colors, respectively.

3.3. The Regulating Effects of Xylem Conductance

The second set of numerical experiments investigated the extent to which the water use strategy can be modified in the model through gradual changes over a wide spectrum of k_{max} values. The 'optimal' k_{max} was selected based on the minimum mean absolute error (MAE) with respect to the upscaled E_T values. Figure 5 illustrates that moving from high k_{max} (Hk_{max}) towards the low k_{max} (Lk_{max}) configuration, the simulated transpiration can be 'adjusted' to capture the differences in transpiration seasonality at the four selected sites. The Hk_{max} and intermediate high

390   k_{max} (IHk_{max}) did not show differences in the simulated E_T for the selected sites, as within this
391   range of k_{max} values transpiration rates are limited by the atmospheric water demand. Most
392   effective changes in the simulated E_T values occur in the range between the default k_{max} (DCk_{max})
393   and low k_{max} (Lk_{max}), with the best correspondence between observed sap flow and simulated
394   transpiration rates achieved by the DCk_{max} at FR-Hes, and the ILk_{max} for the other sites. Here it is
395   interesting to note that at ES-Alt, the model performances can be further improved by increasing
396   the sampled k_{max} values between ILk_{max} and Lk_{max} (see Figure S4), with an 'optimal' k_{max} value
397   of 6.5×10^{-8} mm$_{H2O}$ mm$_{H2O}^{-1}$s^{-1}.

398   We found that gradual changes in k_{max} systematically affected soil evaporation across all
399   sites, where soil evaporation increased from Hk_{max} towards Lk_{max} (Figure 5). These effects are
400   visible at the top 12 cm of soil (first three layers), where the model allocates 34 % of the root
401   biomass. This tendency shows the impact of transpiration on the soil water reservoir by
402   increasing the plant water acquisition. Higher k_{max} values allow extracting more water from the
403   soil and hence reducing the soil moisture. In contrast, reduced k_{max} compared to the default value
404   result in a reduced water transport capacity and diminishing soil water acquisition. As a result,
405   when k_{max} is smaller than DC, soil evaporation increases considerably at all sites (Figure 5). The
406   Lk_{max} configuration restricts the plant water transport at all sites to a point where the soil matric
407   potential is close to 0 all year round (Figure S3), allowing the soil to evaporate more water while
408   transpiration rates are reduced. For the evergreen sites (i.e., FR-Pue and ES-Alt), the Lk_{max}
409   configuration makes soil water to evaporate at high rates, even matching the transpiration
410   measured in summer at FR-Pue and similar values all year round at ES-Alt.

411   Sites covered with *Fagus sylvatica* do not experience extreme transpiration stress ($\beta<0.5$)
412   even when the E_T is overestimated as in the Hk_{max}, IHk_{max}, and DC configurations. The
413   increment of leaf water stress with the Lk_{max} configuration at these two sites (i.e., FR-Hes and
414   DE-Hin) does not go beyond 0.5. This is the consequence of the limited water transport within
415   the plant, impacting the stomatal conductance used to determine the β values. The sites with
416   *Quercus ilex* (i.e., FR-Pue and ES-Alt) experience a more significant leaf water stress in summer
417   when the k_{max} overestimates the transpiration in spring (Hk_{max}, IHk_{max}, and DC). The use of
418   smaller k_{max} values at these drier sites triggers a more restricted vegetation water use under wet
419   conditions (i.e., spring and early summer). Using a smaller k_{max} at sites with stronger dry seasons
420   enables the vegetation to not use all the water in spring, allowing the soil water reservoir to
421   supply the moisture needed in summer. The most suitable k_{max} at FR-Hes corresponds to the DC.
422   DE-Hin, which has the same tree species as FR-Hes, shared with FR-Pue the ILk_{max} as the best
423   performing k_{max}. This is despite the differences between the two sites in tree species, tree size,
424   and stand age (Table 1). The fact that a similar k_{max} does not characterize the same species points
425   out that xylem conductance can be influenced by factors other than genetics (e.g., environmental
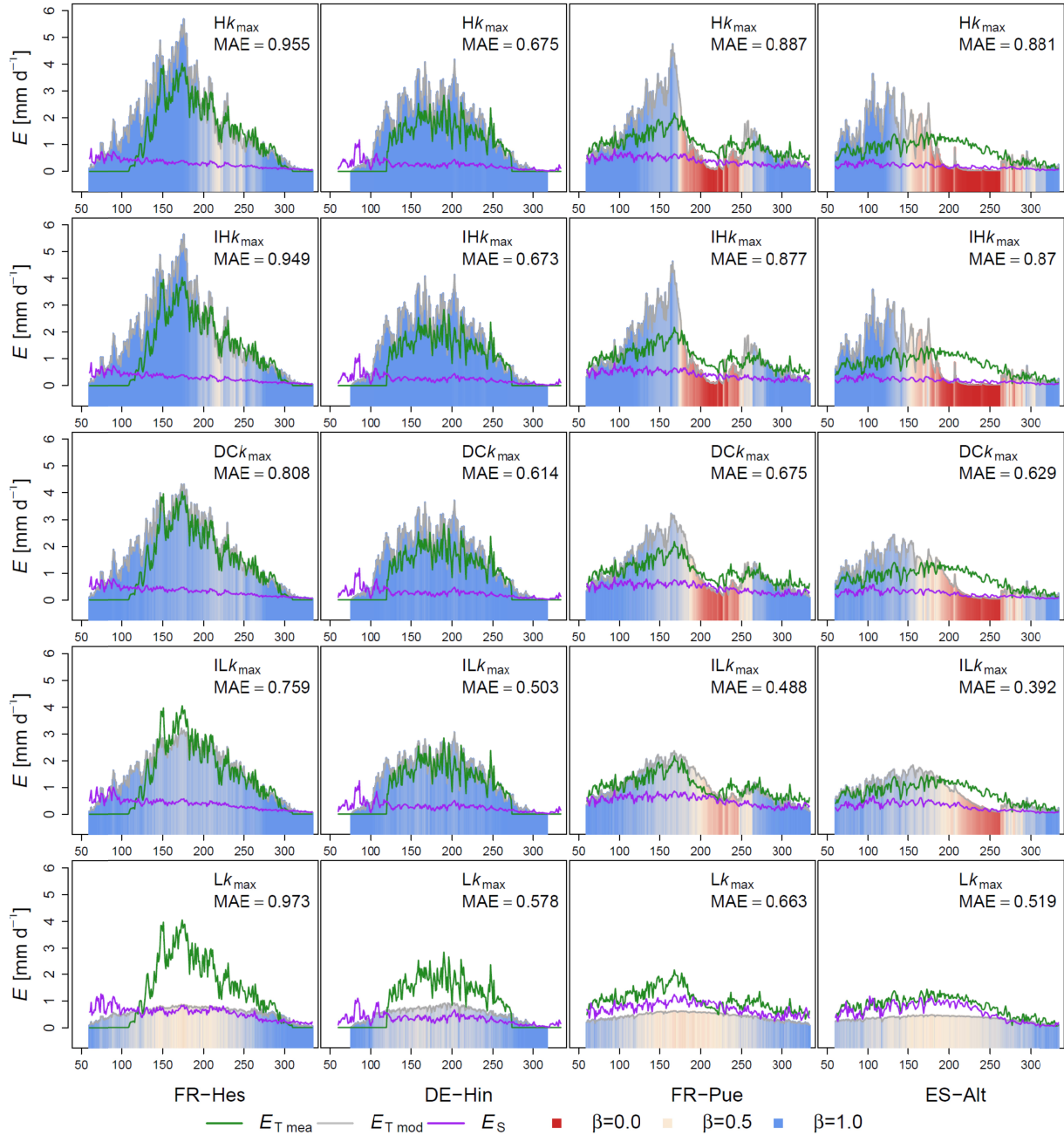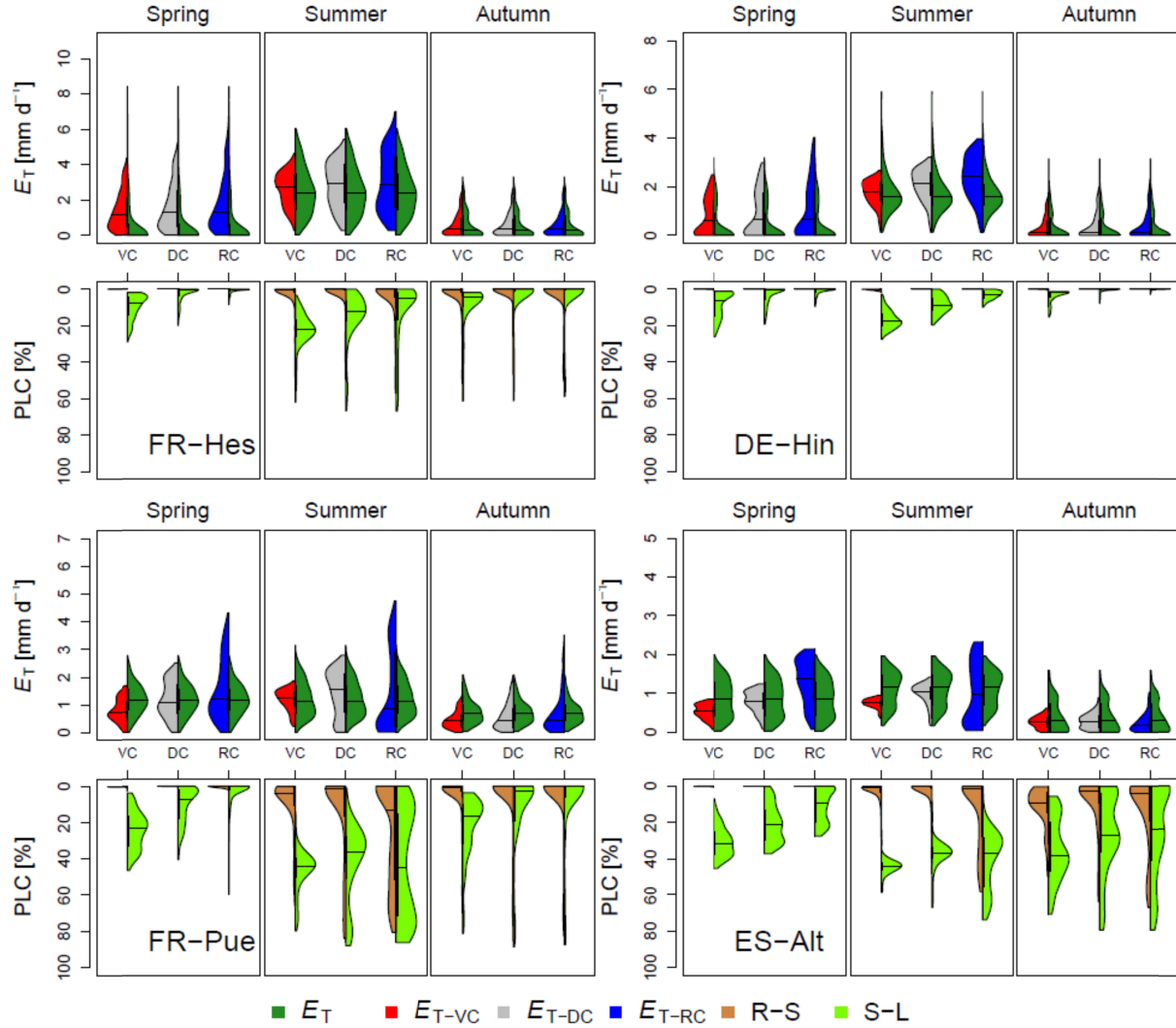426   conditions, growth history).

Figure 5. Temporal variation of transpiration (E_T), soil evaporation (E_S), and leaf water stress factor (β) to gradual changes of maximum xylem conductance (k_{max}) at each experimental site. The plots for each site represent a decrease of maximum xylem conductance from top (larger k_{max}) to bottom (low k_{max}). The leaf water stress (β) in each plot tends towards reddish colors when β falls below 0.5 (extreme stress), while the blueish colors represent unstressed leaf conditions. The MAE is the mean absolute error of the modelled vs. the measured E_T for each configuration per site.

436   3.4. The Combined Effects of Changing the Shape of the Vulnerability Curve and the
437   Maximum Xylem Conductance

438   The third set of experiments was designed to evaluate the sensitivity of E_T to the plant
439   vulnerability curve (PVC) parameters with the modified k_{max}. We expect that the use of best-
440   fitted k_{max} values obtained in the second set of experiments allows a better evaluation of the
441   impacts of the coordinated changes between c_k and Ψ_{p50}. As compared to Figure 1, the simulated
442   E_T is much closer to the observed at all sites for DC, also avoiding extreme stress at xylem level
443   (PLC < 50%) for extended periods (Figure 6). Furthermore, the coordinated changes of the shape
444   parameters with the k_{max} enable the simulation of a more realistic hydraulic response of the root-
445   stem and stem-leaf segment to dry season conditions across the four selected sites (Figure 6).
446   The results indicate that in sites populated by *Fagus sylvatica*, the severe hydraulic failure events
447   (PLC > 50%) simulated by the model are much less frequent at FR-Hes and are completely
448   absent at DE-Hin. Meanwhile, the Mediterranean sites (i.e., FR-Pue and ES-Alt) are
449   characterized by low PLC values (<20 %) for the root-stem plant segment, while more severe
450   PLC values are simulated at the stem-leaf level. Only the RC of these evergreen sites shows a
451   more severe stress response in summer, where the root-stem compartment experiences PLC
452   values larger than 20% for half of the time (second half of the violin plot of Figure 6). At the
453   same time, the xylem-leaf compartment also shows a strong reduction of conductance (PLC >
454   50%). The impact of the RC also affects the xylem-leaf compartment, where the bimodal
455   distribution depicts the problem of the reduced provision of water for vegetation during summer
456   due to a more aggressive soil water extraction in late spring or early summer.

Figure 6. Seasonal response of daily transpiration and loss of hydraulic conductivity to changes in the shape parameters (i.e., Ψ_{p50} and c_k) of the vulnerability curve to hydraulic failure with the best fitted k_{max} at four forested sites in Europe. The distribution of daily transpiration (E_T) and percent loss of conductance (PLC) are represented by seasonal violin plots. The distribution of E_T is contained in the upper plot of each site (solid dark green). The vulnerable (VC), default (DC), and resistant (RC) configurations are represented by red, grey, and blue solid colors, respectively.

4. Discussion

4.1. What is known about the tree species selected?

Fagus sylvatica and *Quercus ilex* are two tree species with contrasting responses to dry periods. These responses depend on physiological adaptations and the cumulative exposure to specific environmental conditions that shape the WUS of each species. *Fagus sylvatica* relies on a small water reservoir because of its shallow root system (Houston Durrant et al., 2016; Kirchen et al., 2017; Leuschner, 2020). This has been documented at FR-Hes and DE-Hin (Granier et al.,

472 2000; Heinrich et al., 2018), where the species were found to be more susceptible to reductions
473 of soil water availability due to dry spells and droughts. This tree species prefers to grow under
474 favorable climatic conditions with abundant precipitation and no water stagnation or prolonged
475 dry periods (Houston Durrant et al., 2016; von Wuehlisch, 2008). This could be why *Fagus*
476 *sylvatica,* keeps significant transpiration rates as leaf water potentials decline, but it is also
477 frequently observed to shed leaves prematurely under extreme drought, which could be to reduce
478 water loss and hydraulic failure or due to hydraulic failure (Leuschner, 2020).

479   *Quercus ilex* can grow deep roots, increasing the accessible water reservoir and allowing
480 the trees to withstand long dry periods (Peñuelas & Filella, 2003; Zapater et al., 2011), as has
481 been shown at FR-Pue and ES-Alt (Baldocchi et al., 2010; Forner et al., 2018). Its evergreen
482 character is maintained during summer thanks to its physiological adaptations such as
483 sclerophyllous leaves, summer growth reduction, and strong stomatal control (Barbeta &
484 Peñuelas, 2016; Terradas & Savé, 1992). The high wood density of oak is linked to its reduced
485 porosity, allowing it to resist lower matric potentials during summer, reducing its susceptibility
486 to hydraulic failure (Terradas & Savé, 1992). The strong stomatal control of this species
487 classifies it as the most isohydric species of the *Quercus* genus (Barbeta & Peñuelas, 2016). This
488 process is clearly visible in summer at FR-Pue and ES-Alt, where precipitation is scarce, and the
489 trees reduce transpiration rates by closing their stomata. Overall, the difference between the two
490 selected species relies on the degree of vulnerability to hydraulic failure and the WUS, with
491 *Fagus sylvatica* showing a vulnerable response and aggressive WUS, while *Quercus ilex* is more
492 resistant to hydraulic failure with a conservative WUS.

493   4.2. Some unexpected effects of the vulnerability curve shape parameters

494   The pant vulnerability curve (PVC) is widely used to model the plant water use response
495 to water stress from single trees up to the ecosystem scales (Kennedy et al., 2019; Li et al., 2021;
496 Mackay et al., 2015; Mencuccini et al., 2019; Sloan et al., 2021). To our knowledge, the impact
497 of characterizing the shape parameters of the curve (Ψ_{p50} and c_k) for the different species or plant
498 functional types (PFTs) has not been investigated in detail for the current implementations of the
499 PVC in land surface models (LSMs). In CLM5, the default parameterization of the plant
500 hydraulic traits is the same for the PFTs under analysis at the four experimental sites. This
501 provided the opportunity to evaluate the effect of the environmental conditions, namely the
502 dynamics of atmospheric water demand and soil water availability, on the simulated plant
503 hydraulic response. FR-Hes and DE-Hin are sites with a continuous water supply during summer
504 due to the low intra-seasonal variability of precipitation (Blume et al., 2022; Granier et al.,
505 2008). Regular precipitation prevents the drying out of the soil water reservoir during summer,
506 allowing the vegetation to operate at low to moderate levels of water stress throughout the year.
507 The default plant hydraulic parameterization of CLM5 reproduces an aggressive water use
508 strategy (WUS) of *Fagus sylvatica* at FR-Hes, allowing the vegetation to transpire at rates close
509 to the atmospheric water demand. However, the use of the same plant hydraulic parameterization
510 across the selected PFTs (Table 2) does not reflect the conservative WUS expected at
511 Mediterranean sites, such as FR-Pue and ES-Alt, which are inhabited by *Quercus ilex*. These two
512 sites have a strong atmospheric water demand but receive very little precipitation in summer
513 (Allard et al., 2008; Lorenzo-Lacruz et al., 2010), resulting in extremely negative soil water
514 potentials and severe plant water stress in the default model simulations (Jiménez-Rodríguez et
515 al., 2022). Although inclusion of water uptake from deeper soil reservoirs can reduce the severity
516 of simulated water stress and under-estimation of transpiration rates in the model (Jiménez-

517 Rodríguez et al., 2022), here we found that reducing the plant hydraulic conductance can
518 improve both, the over-estimation of transpiration in the early growing season and the under-
519 estimation in late summer, due to more carry-over soil resources from the early to the late
520 season.

521   The limitations underscored by the default plant hydraulic parameterization of CLM5 in
522 reproducing the aggressive and conservative WUS persist when changes are applied only to the
523 Ψ_{p50} and c_k parameters. That is, the model response is dominated by the instantaneous
524 atmospheric water demand and restricted by the soil water availability. Therefore, at sites where
525 water supply is continuous throughout the year (e.g., FR-Hes and DE-Hin) the decrease of Ψ_{p50}
526 with the resistant configuration (RC) allows more water to be extracted under given
527 meteorological conditions while reducing plant water stress (PLC and β) as expected (Knüver et
528 al., 2022; Walthert et al., 2021). However, the RC overestimates transpiration rates (E_T) for both
529 sites (Figure 4 and Figure S1). This pattern of the model response illustrates the dominant role of
530 plant hydraulics over stomatal control of E_T. Under seasonally limited soil water supply, as is the
531 case at FR-Pue and ES-Alt during summer, the model simulates a counter-intuitive response
532 when changing the shape parameters of the PVC, with the resistant configuration (RC) suffering
533 more water stress and a reduced E_T than the default or vulnerable configurations (DC and VC,
534 respectively) (Figure 4). The entire intraspecific variability in PVC shape parameters for
535 *Quercus ilex* does not reproduce the conservative WUS in the model that would be expected of a
536 tree species able to withstand significant water shortage conditions (Barbeta & Peñuelas, 2016;
537 Terradas & Savé, 1992). In the contrary, the choice of more resistance PVC shape parameters
538 diminished soil water availability simulated at FR-Pue and ES-Alt during summer due to over-
539 use of water in spring, magnifying the overall vegetation water stress.

540   4.3. Uncovering the role of maximum xylem conductance

541   The results of the second set of numerical experiments highlight the role of the maximum
542 xylem conductance (k_{max}) in determining the transpiration rates under ample water supply and
543 therefore shaping the seasonal water use strategy. The presented results illustrate the effective
544 role of k_{max} in constraining the water use at sites with seasonal water limitations (i.e., FR-Pue and
545 ES-Alt). The maximum specific hydraulic conductance is a parameter highly influenced by local
546 environmental conditions rather than genetics (Hochberg et al., 2018; Lu et al., 2022). This
547 characteristic is represented by the range of k_{max} values observed for the same species (Figure
548 S5). The observed k_{max} values vary by two orders of magnitude for *Fagus sylvatica* (BDT) and
549 five orders of magnitude for *Quercus ilex* (BET), with similar maximum values for both. The
550 primary role of k_{max} for the plant hydraulic system of CLM5 is in constraining the water transport
551 during unstressed conditions and thereby determining the magnitude of plant water use and how
552 much water is left in the ground, some of which might be available later. At FR-Hes, larger k_{max}
553 values compared to the default value increase the water transport in the model, allowing to match
554 the atmospheric water demand and observations. In contrast, smaller k_{max} values are needed at
555 ES-Alt and FR-Pue to prevent the vegetation from depleting the soil water reservoir in spring
556 and therefore enable continued plant water use under moderate stress during the dry summer. A
557 lower k_{max} depicts a transport limitation allowing to reduce the water stress on the plant in the
558 model, while a larger k_{max} allows the model to transpire at higher rates, mimicking an aggressive
559 WUS. CLM5 differs from other numerical models that rely on stomatal conductance to control
560 or mimic the WUS (Sloan et al., 2021). Therefore, in CLM5, an adequate selection of k_{max} plays
561 the role of restraining the vegetation from transpiring excessively in spring and at the beginning

562 of summer to ensure an adequate water supply as summer progresses in a Mediterranean
563 (summer-dry) climate. Note that in the Darcy's law equation used in the plant hydraulics system
564 of CLM5 a certain sensitivity in the simulated transpiration fluxes could be expected by
565 changing also the cross-sectional area of the different plant segments (e.g., SAI). However, there
566 is not a direct correspondence between the prescribed SAI values in the model (defined as the
567 sum of all non-photosynthetic vegetation, including stems, branches, and dead leaves (P. J.
568 Lawrence & Chase, 2007)) and the basal area reported from the selected sites (Table 1), which
569 adds uncertainty in the simulated transpiration fluxes.

570 Most models describe the plant vascular factor by lumping the entire system into a single
571 term (Fatichi et al., 2016), omitting the large variability of the forest ecosystems related to tree
572 species and age (Weithmann et al., 2022). This is the case for k_{max} within the plant hydraulic
573 system of CLM5, where the default k_{max} value is commonly used, disregarding the variability of
574 different tree species and stand density within the PFT classification. Previous studies argue that
575 k_{max} expresses the maximum xylem specific conductance of vegetation under the most favorable
576 environmental conditions (Sabot et al., 2020) and its determination depends on the measurements
577 of specific xylem conductance (k_s), which is a key plant hydraulic trait contributing to the control
578 of the water transport capacity of vegetation (Eamus et al., 2016). This plant hydraulic trait
579 (PHT) varies accordingly with the plant species, environmental conditions, and tree size
580 (Anfodillo & Olson, 2021; Domec et al., 2012; Domec Jean-Christophe et al., 2008; Hochberg et
581 al., 2018; Willigen et al., 2000).

582 The use of plant hydraulics in land surface modelling provides a framework to connect
583 the environmental conditions with the stomatal response (Venturas et al., 2017), allowing a better
584 control on the simulated plant water use strategies. However, we found that the site-specific
585 character of k_{max} has largely been ignored by the modelling community. The default value for
586 k_{max} is the same for all PFTs, and an order of magnitude lower than the lowest reported specific
587 xylem conductance (k_s) for *Fagus sylvatica*, whereas the reported values for *Quercus ilex* have
588 two outliers, one and three orders of magnitude below the default value (see Figure S5 for more
589 details). The k_s values of *Fagus sylvatica* do not match the range of k_{max} used in the second
590 experiment, where the high xylem conductance (Hk_{max}) is close to the lowest k_s value found for
591 this tree species. However, we found little difference in the simulations between the highest
592 values of k_{max}, so exploring the range of values where most observations lie would not improve
593 the model simulations. The differences between the reported k_s and model-default k_{max}
594 highlights the complexity of defining the k_{max} value for different plant functional types (PFTs)
595 based on experimental data with a larger number of species. Here we show how important is the
596 correct parametrization of k_{max} in CLM5 for capturing the water use by vegetation in summer-dry
597 climates. To progress, we need a better understanding of how k_{max} is controlled by a complex set
598 of growing conditions and co-ordination between the root system and leaf area index (Aranda et
599 al., 2015; Lemoine et al., 2002).

600

601 4.4. Understanding the impact of coordinated changes of plant hydraulic traits in CLM5

602 We found that the adjustment of the hydraulic vulnerability curve shape parameters (Ψ_{p50}
603 and c_k) alone did not enable the reproduction of the observed water use dynamics (Figure 4), as
604 choosing a parameterization that is more resistant to hydraulic failure (RC) resulted in even more
605 reduced dry season water use, if the maximum hydraulic conductance (k_{max}) was too high.

606 Indeed, the drastic effect caused by the more negative Ψ_{p50} of the RC is diminished by using a
607 smaller k_{max}, reducing the water extraction in spring, and letting the vegetation experience lower
608 PLC values in summer (Figure 6). Also, the fact that the VC of *Fagus sylvatica* results in low
609 PLC for the root-stem and more severe PLC for stem-leaf shows the model's ability to reproduce
610 important physiological processes along the PLC curve (Huber et al., 2019). These processes
611 may trigger different drought survival strategies depending on the species. For *Fagus sylvatica*,
612 water stress and loss in conductance may result in premature shedding of leaves during dry
613 conditions (Arend et al., 2022) or stomatal closure (Schuldt et al., 2016). The sites populated by
614 *Quercus ilex* are better simulated using low k_{max} values (Figures 5 and S4), which allow to better
615 reproduce the WUS of species adapted to water scarce environments (Terradas & Savé, 1992).
616 Nonetheless, extremely low Ψ_{p50} still trigger an excessive water uptake during the driest part of
617 the summer at Mediterranean sites (Figure 6), demonstrating the lack of stomatal regulation in
618 the model and its strong dependency on hydraulic limitations and soil water availability to
619 control the magnitude of E_T. Note that in our study, k_{max} was selected based on the default
620 vulnerability curve shape parameters, whereas the latter were adjusted in a second step, using the
621 previously selected k_{max}. The results could likely be improved by choosing an optimal
622 combination of k_{max}, Ψ_{p50} and c_k, but model calibration is not the goal of the present study.

623 The results of our study also demonstrate that generalizing the use of k_{max} as a
624 homogeneous parameter across PFTs in CLM5 prevents an adequate reproduction of the
625 magnitude and timing of E_T at sites in different climates. Also, the independence between
626 stomatal control and hydraulic conductance in the model is contradictory to what the existing
627 evidence suggests (Franks, 2004). These aspects magnify the effect that more negative Ψ_{p50} has
628 on the water extraction when we change only the curve shape parameters, something that was
629 overlooked in previous studies (e.g., Bai et al. (2021), Song et al. (2020)). The results of the
630 coordinated changes in safety (i.e., the shape parameters Ψ_{p50} and c_k) and efficiency (i.e., k_{max})
631 hydraulic traits underline how k_{max} rules the WUS in the model, while Ψ_{p50} and c_k modulate the
632 level of the hydraulic stress experienced. An adequate parameterization of k_{max}, Ψ_{p50} and c_k in
633 combination is critical for obtaining a simulated plant hydraulic response that conforms with the
634 plant water supply theory and the expected physiological response of vegetation subjected to dry
635 conditions.

636 4.5. Addressing the plant hydraulic traits: homogeneity versus diversity

637 The plant functional type (PFT) classification system has been a valuable tool for
638 understanding drought resilience from an ecosystem perspective (Sturm et al., 2022). However,
639 the large variation in ecosystem functional properties related to the water cycle is insufficiently
640 explained by this classification system (Reichstein et al., 2014). Skelton et al. (2015) stressed the
641 need to characterize the plant response to drought by merging the current knowledge of the water
642 use strategies (WUS) with the xylem vulnerability. To fulfill this need, this classification system
643 requires the characterization of the physiological traits per vegetation type and growing stage.
644 Nonetheless, these aspects are heavily homogenized using the current PFT classification system,
645 affecting the capacity to correctly predict the ecosystem water use (Konings & Gentine, 2017)
646 and leading to a poor predictive skill of the vulnerability to hydraulic failure.

647 *Fagus sylvatica* and *Quercus ilex* represent part of the variability of the plant hydraulic
648 traits (PHT) within the broadleaf deciduous (BDT) and broadleaf evergreen (BET) PFT classes.
649 Aiming to provide a broader context of the role of homogeneity versus diversity in plant

650 hydraulic trait studies, we sampled the XFT database (Choat et al., 2012) for a preselected set of
651 species per PFT in Europe (Buras & Menzel, 2019; Fyllas et al., 2020; Leuschner & Meier,
652 2018) with the emphasis placed on the temperate BDT, BET, and adding the needleleaf
653 evergreen (NET) PFT to enrich the analysis (see Table S2 for details of the sampled species).
654 Figure 7 illustrates that the Ψ_{p50} used by default in CLM5 fails to capture the values of Ψ_{p50} for
655 NET and BDT in Europe, as the default values are not even close to the median values of the
656 distributions. The Ψ_{p50} of NET in CLM5 is way beyond the Ψ_{p88} for this PFT, representing an
657 extremely resistant tree with respect to the published data, while the Ψ_{p50} of BDT depicts a more
658 vulnerable tree closer to the reported median of Ψ_{p12}. The default Ψ_{p50} of BET in CLM5 matches
659 the median of the published data, but the large range showed by this PFT (-0.5 MPa to -9 MPa)
660 raises the question of how much of this variability is driven by geography or environmental
661 conditions. An even more important aspect to be considered is an adequate selection of k_{max} for
662 the PFTs, where the large variability showed for individual species does not agree with the best
663 fitted k_{max} of the model. This finding depicts the issue of considering k_{max} as constant among
664 PFTs when the variability of the species describing these PFTs is large (see Figure S5).

665 Liu et al. (2020) showed the benefit of considering the plant hydraulics in LSMs, where
666 the overestimation of vegetation water use is a common issue. They also recognize the ability of
667 plant hydraulics to predict vulnerability to droughts. In this regard, Kennedy et al. (2019)
668 introduced the plant water stress routine in CLM5 that compartmentalized the PHT according to
669 PFT type. From an ecosystem perspective, simplifying hydraulic traits into single plant
670 functional types has additional repercussions. Matheny (2021) highlighted the importance of
671 incorporating flexible traits based on prevalent environmental stressors since tree species'
672 sensitivity to water stress is determined by their plasticity to the environment (Haberstroh &
673 Werner, 2022). This plasticity is exemplified by the different k_{max} values in *Fagus sylvatica* and
674 *Quercus ilex* in this manuscript, and the reported variability of xylem specific conductance
675 reported across many orders of magnitude for each species (e.g., Bär et al., 2018; Carevic et al.,
676 2014; Charra-Vaskou et al., 2012; Choat et al., 2012; David et al., 2007; Limousin et al., 2010;
677 Lübbe et al., 2022; Martínez-Vilalta et al., 2002; Tomasella et al., 2019). Flexible traits based on
678 the environmental stressors in CLM5 can be used by the spectrum of PVCs per PFT and
679 exploiting the role of k_{max} in regulating the WUS in the model. By adjusting the k_{max} to better
680 represent the transpiration response we may be able to identify the timing of important
681 physiological processes (e.g., leaf shedding) that differ between the VC and RC. In this way, we
682 may be able to better understand the significant changes in different ecosystem processes
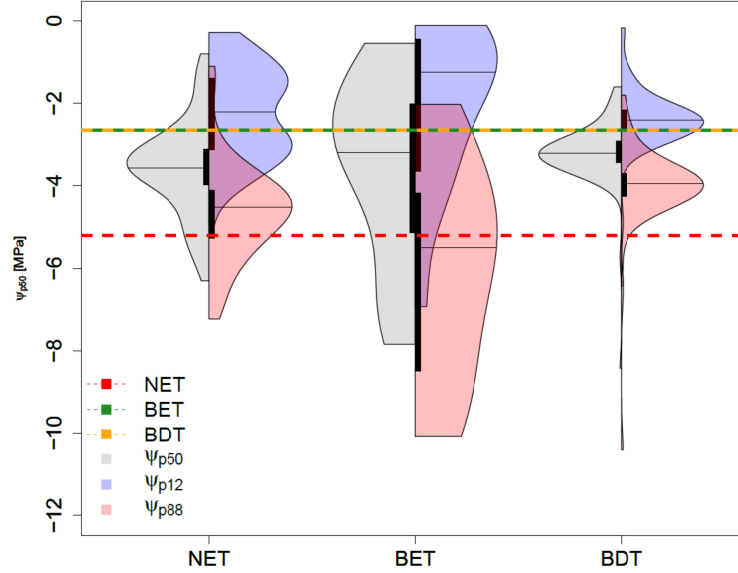683 triggered by intense dry periods (Oddi et al., 2022).

Figure 7. Violin plots describing the variability of the plant hydraulic traits (Ψp12, Ψp50, and Ψp88) within broadleaf evergreen (BET), broadleaf deciduous (BDT), and needleleaf evergreen (NET) trees plant functional types (PFTs) representative of European forests (see Table S2 for the list of pre-selected tree species per PFT). The red, green, and yellow dashed lines represent the NET, BET, and BDT default values of Ψp50 used by CLM5, respectively.

5 Conclusions

The intraspecific variability of the plant hydraulic traits of individual plant functional types (PFT) allows to describe the spectrum of vulnerability to hydraulic failure from vulnerable to resistant responses of different tree species. Understanding the importance of the right selection of k_{max}, Ψ_{p50} and c_k from their large within-species variation requires a detailed understanding of the role played within the model. This information is crucial for the modelling community, where the parameter selection may induce considerable bias when assuming that all tree species within the same PFT behave equally in different environmental conditions. The adequate identification of dominant tree species per experimental site allows to narrow down the variability of multiple species or by weighing the tree species contribution within the PFT, but given the large variability in hydraulic traits even within a single species, a large uncertainty prevails. Adjustments of the shape parameters of the hydraulic vulnerability curve (Ψ_{p50} and c_k) alone do not enable the model to reproduce E_T during spring and summertime at sites with seasonal water deficits. The seasonal differences between measured and modelled transpiration illustrate the importance of the maximum plant hydraulic conductance (k_{max}) for controlling the magnitude and timing of E_T, i.e. the general water use strategy (WUS). A larger k_{max} allows the trees to transpire larger amounts of water during favorable water conditions, quickly depleting the soil water reservoir. In contrast, smaller k_{max} values limit the water transport and hence soil water extraction rates, pushing the vegetation towards a more conservative WUS. Consequently, k_{max} is a significant player in controlling the transpiration in CLM5 and allowing to mimic the WUS of different species by limiting or enhancing the water transport. However, given the large within-species variability in k_{max}, more research is needed to enable adequate parameterization of the site-specific k_{max}. This work reveals the potential of plant hydraulic traits to mimic aggressive

713 or conservative WUS in CLM5, crucial for adequate reproduction of plant water use dynamics in
714 different climates. Given the large intra-specific variation in plant hydraulic traits and the
715 importance of the stand characteristics (e.g., tree height, stem area index) for limiting
716 transpiration rates in the model, a more fundamental understanding of the drivers for adjustments
717 in these parameters is needed.

Acknowledgments

721

Open Research

723 The SAPFLUXNET data used for atmospheric forcing and transpiration estimates in the study
724 are available at ZENODO repository via https://doi.org/10.5281/zenodo.3971689 with a Creative
725 Commons Attribution 4.0 International license for the files. The COSMO-REA6 data used to
726 complete the missing data for the atmospheric forcing in the study are available from the
727 opendata-FTP server at DWD
728 (https://opendata.dwd.de/climate_environment/REA/COSMO_REA6/).

729

References

731 Allard, V., Ourcival, J. M., Rambal, S., Jofre, R., & Rocheteau, A. (2008). Seasonal and annual

732 variation of carbon exchange in an evergreen Mediterranean forest in southern France.

733 *Global Change Biology*, *14*(4), 714–725. https://doi.org/10.1111/j.1365-

734 2486.2008.01539.x

735 Allen, R. G., Pereira, L. S., Raes, D., & Smith, M. (1998). *Crop evapotranspiration-Guidelines for*

736 *computing crop water requirements-FAO Irrigation and drainage paper 56*. FAO - Food

737 and Agriculture Organization of the United Nations.

738 An, N., Hemmati, S., & Cui, Y.-J. (2017). Assessment of the methods for determining net radiation

739 at different time-scales of meteorological variables. *Journal of Rock Mechanics and*

740 *Geotechnical Engineering*, *9*(2), 239–246. https://doi.org/10.1016/j.jrmge.2016.10.004

741   Anfodillo, T., & Olson, M. E. (2021). Tree Mortality: Testing the Link Between Drought, Embolism

742   Vulnerability, and Xylem Conduit Diameter Remains a Priority. *Frontiers in Forests and*

743   *Global Change*, *4*. https://www.frontiersin.org/articles/10.3389/ffgc.2021.704670

744   Aranda, I., Cano, F. J., Gascó, A., Cochard, H., Nardini, A., Mancha, J. A., López, R., & Sánchez-

745   Gómez, D. (2015). Variation in photosynthetic performance and hydraulic architecture

746   across European beech (Fagus sylvatica L.) populations supports the case for local

747   adaptation to water stress. *Tree Physiology*, *35*(1), 34–46.

748   https://doi.org/10.1093/treephys/tpu101

749   Arend, M., Link, R. M., Zahnd, C., Hoch, G., Schuldt, B., & Kahmen, A. (2022). Lack of hydraulic

750   recovery as a cause of post-drought foliage reduction and canopy decline in European

751   beech. *New Phytologist*, *234*(4), 1195–1205. https://doi.org/10.1111/nph.18065

752   Bai, Y., Liu, Y., Kueppers, L. M., Feng, X., Yu, K., Yang, X., Li, X., & Huang, J. (2021). The coupled

753   effect of soil and atmospheric constraints on the vulnerability and water use of two

754   desert riparian ecosystems. *Agricultural and Forest Meteorology*, *311*, 108701.

755   https://doi.org/10.1016/j.agrformet.2021.108701

756   Baldocchi, D. D., Ma, S., Rambal, S., Misson, L., Ourcival, J.-M., Limousin, J.-M., Pereira, J., &

757   Papale, D. (2010). On the differential advantages of evergreenness and deciduousness in

758   mediterranean oak woodlands: A flux perspective. *Ecological Applications*, *20*(6), 1583–

759   1597. https://doi.org/10.1890/08-2047.1

760   Bär, A., Nardini, A., & Mayr, S. (2018). Post-fire effects in xylem hydraulics of Picea abies, Pinus

761   sylvestris   and   Fagus   sylvatica.   *New   Phytologist*,   *217*(4),   1484–1493.

762   https://doi.org/10.1111/nph.14916

763 Barbeta, A., & Peñuelas, J. (2016). Sequence of plant responses to droughts of different

764   timescales: Lessons from holm oak (Quercus ilex) forests. *Plant Ecology & Diversity*, *9*(4),

765   321–338. https://doi.org/10.1080/17550874.2016.1212288

766 Beck, H. E., Zimmermann, N. E., McVicar, T. R., Vergopolan, N., Berg, A., & Wood, E. F. (2018).

767   Present and future Köppen-Geiger climate classification maps at 1-km resolution.

768   *Scientific Data*, *5*(1), 180214. https://doi.org/10.1038/sdata.2018.214

769 Blume, T., Schneider, L., & Güntner, A. (2022). Comparative analysis of throughfall observations

770   in six different forest stands: Influence of seasons, rainfall- and stand characteristics.

771   *Hydrological Processes*, *36*(3), e14461. https://doi.org/10.1002/hyp.14461

772 Bollmeyer, C., Keller, J. D., Ohlwein, C., Wahl, S., Crewell, S., Friederichs, P., Hense, A., Keune, J.,

773   Kneifel, S., Pscheidt, I., Redl, S., & Steinke, S. (2015). Towards a high-resolution regional

774   reanalysis for the European CORDEX domain. *Quarterly Journal of the Royal*

775   *Meteorological Society*, *141*(686), 1–15. https://doi.org/10.1002/qj.2486

776 Bonan, G. B., Levis, S., Kergoat, L., & Oleson, K. W. (2002). Landscapes as patches of plant

777   functional types: An integrating concept for climate and ecosystem models. *Global*

778   *Biogeochemical Cycles*, *16*(2), 5–1. https://doi.org/10.1029/2000GB001360

779 Buras, A., & Menzel, A. (2019). Projecting Tree Species Composition Changes of European

780   Forests for 2061–2090 Under RCP 4.5 and RCP 8.5 Scenarios. *Frontiers in Plant Science*, *9*.

781   https://www.frontiersin.org/articles/10.3389/fpls.2018.01986

782 Butler, E. E., Wythers, K. R., Flores-Moreno, H., Ricciuto, D. M., Datta, A., Banerjee, A., Atkin, O.

783   K., Kattge, J., Thornton, P. E., Anand, M., Burrascano, S., Byun, C., Cornelissen, J. H. C.,

784   Forey, E., Jansen, S., Kramer, K., Minden, V., & Reich, P. B. (2022). Increasing Functional

785   Diversity in a Global Land Surface Model Illustrates Uncertainties Related to Parameter

786   Simplification. *Journal of Geophysical Research: Biogeosciences*, *127*(3), e2021JG006606.

787   https://doi.org/10.1029/2021JG006606

788   Carevic, F., Fernández, M., Alejano, R., & Vázquez-Piqué, J. (2014). Xylem cavitation affects the

789   recovery of plant water status and consequently acorn production in a holm oak open

790   woodland.   *Acta   Physiologiae   Plantarum*,   *36*(12),   3283–3290.

791   https://doi.org/10.1007/s11738-014-1694-6

792   Charra-Vaskou, K., Charrier, G., Wortemann, R., Beikircher, B., Cochard, H., Ameglio, T., & Mayr,

793   S. (2012). Drought and frost resistance of trees: A comparison of four species at different

794   sites   and   altitudes.   *Annals   of   Forest   Science*,   *69*(3),   325–333.

795   https://doi.org/10.1007/s13595-011-0160-5

796   Choat, B., Jansen, S., Brodribb, T. J., Cochard, H., Delzon, S., Bhaskar, R., Bucci, S. J., Feild, T. S.,

797   Gleason, S. M., Hacke, U. G., Jacobsen, A. L., Lens, F., Maherali, H., Martínez-Vilalta, J.,

798   Mayr, S., Mencuccini, M., Mitchell, P. J., Nardini, A., Pittermann, J., … Zanne, A. E. (2012).

799   Global convergence in the vulnerability of forests to drought. *Nature*, *491*(7426), 752–

800   755. https://doi.org/10.1038/nature11688

801   Christoffersen, B. O., Gloor, M., Fauset, S., Fyllas, N. M., Galbraith, D. R., Baker, T. R., Kruijt, B.,

802   Rowland, L., Fisher, R. A., Binks, O. J., Sevanto, S., Xu, C., Jansen, S., Choat, B., Mencuccini,

803   M., McDowell, N. G., & Meir, P. (2016). Linking hydraulic traits to tropical forest function

804   in a size-structured and trait-driven model (TFS v.1-Hydro). *Geosci. Model Dev.*, *9*(11),

805   4227–4255. https://doi.org/10.5194/gmd-9-4227-2016

806 David, T. S., Henriques, M. O., Kurz-Besson, C., Nunes, J., Valente, F., Vaz, M., Pereira, J. S.,

807   Siegwolf, R., Chaves, M. M., Gazarini, L. C., & David, J. S. (2007). Water-use strategies in

808   two co-occurring Mediterranean evergreen oaks: Surviving the summer drought. *Tree*

809   *Physiology*, *27*(6), 793–803. https://doi.org/10.1093/treephys/27.6.793

810 de Rigo, D., & Caudullo, G. (2016). Quercus ilex in Europe: Distribution, habitat, usage and

811   threats. In *European Atlas of Forest Tree Species*. Publication Office of the European

812   Union. https://forest.jrc.ec.europa.eu/en/european-atlas/atlas-download-page/

813 Deng, L., Peng, C., Kim, D.-G., Li, J., Liu, Y., Hai, X., Liu, Q., Huang, C., Shangguan, Z., & Kuzyakov,

814   Y. (2021). Drought effects on soil carbon and nitrogen dynamics in global natural

815   ecosystems. *Earth-Science Reviews*, *214*, 103501.

816   https://doi.org/10.1016/j.earscirev.2020.103501

817 Domec, J.-C., & Gartner, B. L. (2001). Cavitation and water storage capacity in bole xylem

818   segments of mature and young Douglas-fir trees. *Trees*, *15*(4), 204–214.

819   https://doi.org/10.1007/s004680100095

820 Domec, J.-C., Lachenbruch, B., Pruyn, M. L., & Spicer, R. (2012). Effects of age-related increases

821   in sapwood area, leaf area, and xylem conductivity on height-related hydraulic costs in

822   two contrasting coniferous species. *Annals of Forest Science*, *69*(1), 17–27.

823   https://doi.org/10.1007/s13595-011-0154-3

824 Domec Jean-Christophe, Lachenbruch Barbara, Meinzer Frederick C., Woodruff David R., Warren

825   Jeffrey M., & McCulloh Katherine A. (2008). Maximum height in a conifer is associated

826   with conflicting requirements for xylem design. *Proceedings of the National Academy of*

827   *Sciences*, *105*(33), 12069–12074. https://doi.org/10.1073/pnas.0710418105

828 Eamus, D., Huete, A., & Yu, Q. (2016). *Vegetation dynamics. A synthesis of plant ecophysiology,*

829 *remote sensing and modelling.* Cambridge University Press.

830 Eller, C. B., Rowland, L., Oliveira, R. S., Bittencourt, P. R. L., Barros, F. V., da Costa, A. C. L., Meir,

831 P., Friend, A. D., Mencuccini, M., Sitch, S., & Cox, P. (2018). Modelling tropical forest

832 responses to drought and El Niño with a stomatal optimization model based on xylem

833 hydraulics. *Philosophical Transactions of the Royal Society B: Biological Sciences*,

834 *373*(1760), 20170315. https://doi.org/10.1098/rstb.2017.0315

835 Fatichi, S., Pappas, C., & Ivanov, V. Y. (2016). Modeling plant–water interactions: An

836 ecohydrological overview from the cell to the global scale. *WIREs Water*, *3*(3), 327–368.

837 https://doi.org/10.1002/wat2.1125

838 Flo, V., Martínez-Vilalta, J., Mencuccini, M., Granda, V., Anderegg, W. R. L., & Poyatos, R. (2021).

839 Climate and functional traits jointly mediate tree water-use strategies. *New Phytologist*,

840 *231*(2), 617–630. https://doi.org/10.1111/nph.17404

841 Forner, A., Valladares, F., & Aranda, I. (2018). Mediterranean trees coping with severe drought:

842 Avoidance might not be safe. *Environmental and Experimental Botany*, *155*, 529–540.

843 https://doi.org/10.1016/j.envexpbot.2018.08.006

844 Franks, P. J. (2004). Stomatal control and hydraulic conductance, with special reference to tall

845 trees. *Tree Physiology*, *24*(8), 865–878. https://doi.org/10.1093/treephys/24.8.865

846 Fu, Z., Ciais, P., Prentice, I. C., Gentine, P., Makowski, D., Bastos, A., Luo, X., Green, J. K., Stoy, P.

847 C., Yang, H., & Hajima, T. (2022). Atmospheric dryness reduces photosynthesis along a

848 large range of soil water deficits. *Nature Communications*, *13*(1), Article 1.

849 https://doi.org/10.1038/s41467-022-28652-7

850   Fyllas, N. M., Michelaki, C., Galanidis, A., Evangelou, E., Zaragoza-Castells, J., Dimitrakopoulos, P.

851   G., Tsadilas, C., Arianoutsou, M., & Lloyd, J. (2020). Functional Trait Variation Among and

852   Within Species and Plant Functional Types in Mountainous Mediterranean Forests.

853   *Frontiers in Plant Science*, *11*.

854   https://www.frontiersin.org/articles/10.3389/fpls.2020.00212

855   Gleason, S. M., Westoby, M., Jansen, S., Choat, B., Hacke, U. G., Pratt, R. B., Bhaskar, R., Brodribb,

856   T. J., Bucci, S. J., Cao, K.-F., Cochard, H., Delzon, S., Domec, J.-C., Fan, Z.-X., Feild, T. S.,

857   Jacobsen, A. L., Johnson, D. M., Lens, F., Maherali, H., … Zanne, A. E. (2016). Weak

858   tradeoff between xylem safety and xylem-specific hydraulic efficiency across the world's

859   woody plant species. *New Phytologist*, *209*(1), 123–136.

860   https://doi.org/10.1111/nph.13646

861   Granier, A., Bréda, N., Longdoz, B., Gross, P., & Ngao, J. (2008). Ten years of fluxes and stand

862   growth in a young beech forest at Hesse, North-eastern France. *Annals of Forest Science*,

863   *65*(7), 704–704. https://doi.org/10.1051/forest:2008052

864   Granier, A., Ceschia, E., Damesin, C., Dufrêne, E., Epron, D., Gross, P., Lebaube, S., Le Dantec, V.,

865   Le Goff, N., Lemoine, D., Lucot, E., Ottorini, J. M., Pontailler, J. Y., & Saugier, B. (2000).

866   The carbon balance of a young Beech forest. *Functional Ecology*, *14*(3), 312–325.

867   https://doi.org/10.1046/j.1365-2435.2000.00434.x

868   Haberstroh, S., & Werner, C. (2022). The role of species interactions for forest resilience to

869   drought. *Plant Biology*, *n/a*(n/a). https://doi.org/10.1111/plb.13415

870 Hacke, U. G., Sperry, J. S., Wheeler, J. K., & Castro, L. (2006). Scaling of angiosperm xylem

871   structure with safety and efficiency. *Tree Physiology*, *26*(6), 689–701.

872   https://doi.org/10.1093/treephys/26.6.689

873 Hajek, P., Kurjak, D., von Wühlisch, G., Delzon, S., & Schuldt, B. (2016). Intraspecific Variation in

874   Wood Anatomical, Hydraulic, and Foliar Traits in Ten European Beech Provenances

875   Differing in Growth Yield. *Frontiers in Plant Science*, *7*.

876   https://www.frontiersin.org/articles/10.3389/fpls.2016.00791

877 He, X., Pan, M., Wei, Z., Wood, E. F., & Sheffield, J. (2020). A Global Drought and Flood Catalogue

878   from 1950 to 2016. *Bulletin of the American Meteorological Society*, *101*(5), E508–E535.

879   https://doi.org/10.1175/BAMS-D-18-0269.1

880 Heinrich, I., Balanzategui, D., Bens, O., Blasch, G., Blume, T., Böttcher, F., Borg, E., Brademann, B.,

881   Brauer, A., Conrad, C., Dietze, E., Dräger, N., Fiener, P., Gerke, H. H., Güntner, A., Heine,

882   I., Helle, G., Herbrich, M., Harfenmeister, K., … Wilken, F. (2018). Interdisciplinary Geo-

883   ecological Research across Time Scales in the Northeast German Lowland Observatory

884   (TERENO-NE). *Vadose Zone Journal*, *17*(1), 180116.

885   https://doi.org/10.2136/vzj2018.06.0116

886 Hochberg, U., Rockwell, F. E., Holbrook, N. M., & Cochard, H. (2018). Iso/Anisohydry: A Plant–

887   Environment Interaction Rather Than a Simple Hydraulic Trait. *Trends in Plant Science*,

888   *23*(2), 112–120. https://doi.org/10.1016/j.tplants.2017.11.002

889 Houston Durrant, T., de Rigo, D., & Caudullo, G. (2016). Fagus sylvatica and other beeches in

890   Europe: Distribution, habitat, usage and threats. In *European Atlas of Forest Tree Species*.

891   Publication Office of the European Union. https://forest.jrc.ec.europa.eu/en/european-

892   atlas/atlas-download-page/

893 Huber, A. E., Melcher, P. J., Piñeros, M. A., Setter, T. L., & Bauerle, T. L. (2019). Signal

894   coordination before, during and after stomatal closure in response to drought stress.

895   *New Phytologist*, 224(2), 675–688. https://doi.org/10.1111/nph.16082

896 Kennedy, D., Swenson, S., Oleson, K. W., Lawrence, D. M., Fisher, R., Lola da Costa, A. C., &

897   Gentine, P. (2019). Implementing Plant Hydraulics in the Community Land Model, Version

898   5. *Journal of Advances in Modeling Earth Systems*, *11*(2), 485–513.

899   https://doi.org/10.1029/2018MS001500

900 Kirchen, G., Calvaruso, C., Granier, A., Redon, P.-O., Van der Heijden, G., Bréda, N., & Turpault,

901   M.-P. (2017). Local soil type variability controls the water budget and stand productivity

902   in a beech forest. *Forest Ecology and Management*, *390*, 89–103.

903   https://doi.org/10.1016/j.foreco.2016.12.024

904 Klein, T., Zeppel, M. J. B., Anderegg, W. R. L., Bloemen, J., De Kauwe, M. G., Hudson, P., Ruehr, N.

905   K., Powell, T. L., von Arx, G., & Nardini, A. (2018). Xylem embolism refilling and resilience

906   against drought-induced mortality in woody plants: Processes and trade-offs. *Ecological*

907   *Research*, 33(5), 839–855. https://doi.org/10.1007/s11284-018-1588-y

908 Knüver, T., Bär, A., Ganthaler, A., Gebhardt, T., Grams, T. E. E., Häberle, K.-H., Hesse, B. D., Losso,

909   A., Tomedi, I., Mayr, S., & Beikircher, B. (2022). Recovery after long-term summer

910   drought: Hydraulic measurements reveal legacy effects in trunks of Picea abies but not in

911   Fagus sylvatica. *Plant Biology*, *n/a*(n/a). https://doi.org/10.1111/plb.13444

912   Konings, A. G., & Gentine, P. (2017). Global variations in ecosystem-scale isohydricity. *Global*

913   *Change Biology*, *23*(2), 891–905. https://doi.org/10.1111/gcb.13389

914   Lansu, E. M., van Heerwaarden, C. C., Stegehuis, A. I., & Teuling, A. J. (2020). Atmospheric Aridity

915   and Apparent Soil Moisture Drought in European Forest During Heat Waves. *Geophysical*

916   *Research Letters*, *47*(6), e2020GL087091. https://doi.org/10.1029/2020GL087091

917   Lawrence, D. M., Fisher, R. A., Koven, C. D., Oleson, K. W., Swenson, S. C., Bonan, G., Collier, N.,

918   Ghimire, B., van Kampenhout, L., Kennedy, D., Kluzek, E., Lawrence, P. J., Li, F., Li, H.,

919   Lombardozzi, D., Riley, W. J., Sacks, W. J., Shi, M., Vertenstein, M., … Zeng, X. (2019). The

920   Community Land Model Version 5: Description of New Features, Benchmarking, and

921   Impact of Forcing Uncertainty. *Journal of Advances in Modeling Earth Systems*, *11*(12),

922   4245–4287. https://doi.org/10.1029/2018MS001583

923   Lawrence, P. J., & Chase, T. N. (2007). Representing a new MODIS consistent land surface in the

924   Community Land Model (CLM 3.0). *Journal of Geophysical Research: Biogeosciences*,

925   *112*(G1). https://doi.org/10.1029/2006JG000168

926   Lawrence, P. J., & Chase, T. N. (2010). Investigating the climate impacts of global land cover

927   change in the community climate system model. *International Journal of Climatology*,

928   *30*(13), 2066–2087. https://doi.org/10.1002/joc.2061

929   Lemoine, D., Jacquemin, S., & Granier, A. (2002). Beech (Fagus sylvatica L.) branches show

930   acclimation of xylem anatomy and hydraulic properties to increased light after thinning.

931   *Annals of Forest Science*, *59*(7), 761–766. https://doi.org/10.1051/forest:2002062

932   Leuschner, C. (2020). Drought response of European beech (Fagus sylvatica L.)—A review.

933   *Perspectives in Plant Ecology, Evolution and Systematics*, *47*, 125576.

934   https://doi.org/10.1016/j.ppees.2020.125576

935   Leuschner, C., & Meier, I. C. (2018). The ecology of Central European tree species: Trait spectra,

936   functional trade-offs, and ecological classification of adult trees. *Perspectives in Plant*

937   *Ecology, Evolution and Systematics*, *33*, 89–103.

938   https://doi.org/10.1016/j.ppees.2018.05.003

939   Li, L., Yang, Z.-L., Matheny, A. M., Zheng, H., Swenson, S. C., Lawrence, D. M., Barlage, M., Yan, B.,

940   McDowell, N. G., & Leung, L. R. (2021). Representation of Plant Hydraulics in the Noah-

941   MP Land Surface Model: Model Development and Multiscale Evaluation. *Journal of*

942   *Advances in Modeling Earth Systems*, *13*(4), e2020MS002214.

943   https://doi.org/10.1029/2020MS002214

944   Liang, S., Zhang, X., Xiao, Z., Cheng, J., Liu, Q., & Zhao, X. (2014). Leaf Area Index. In S. Liang, X.

945   Zhang, Z. Xiao, J. Cheng, Q. Liu, & X. Zhao (Eds.), *Global LAnd Surface Satellite (GLASS)*

946   *Products: Algorithms, Validation and Analysis* (pp. 3–31). Springer International

947   Publishing. https://doi.org/10.1007/978-3-319-02588-9_2

948   Liang, S., Zhao, X., Liu, S., Yuan, W., Cheng, X., Xiao, Z., Zhang, X., Liu, Q., Cheng, J., Tang, H., Qu,

949   Y., Bo, Y., Qu, Y., Ren, H., Yu, K., & Townshend, J. (2013). A long-term Global LAnd Surface

950   Satellite (GLASS) data-set for environmental studies. *International Journal of Digital Earth*,

951   *6*(sup1), 5–33. https://doi.org/10.1080/17538947.2013.805262

952 Limousin, J.-M., Longepierre, D., Huc, R., & Rambal, S. (2010). Change in hydraulic traits of
953   Mediterranean Quercus ilex subjected to long-term throughfall exclusion. *Tree*
954   *Physiology*, *30*(8), 1026–1036. https://doi.org/10.1093/treephys/tpq062

955 Lindroth, A., Holst, J., Linderson, M.-L., Aurela, M., Biermann, T., Heliasz, M., Chi, J., Ibrom, A.,
956   Kolari, P., Klemedtsson, L., Krasnova, A., Laurila, T., Lehner, I., Lohila, A., Mammarella, I.,
957   Mölder, M., Löfvenius, M. O., Peichl, M., Pilegaard, K., … Nilsson, M. (2020). Effects of
958   drought and meteorological forcing on carbon and water fluxes in Nordic forests during
959   the dry summer of 2018. *Philosophical Transactions of the Royal Society B: Biological*
960   *Sciences*, *375*(1810), 20190516. https://doi.org/10.1098/rstb.2019.0516

961 Liu, Y., Kumar, M., Katul, G. G., Feng, X., & Konings, A. G. (2020). Plant hydraulics accentuates the
962   effect of atmospheric moisture stress on transpiration. *Nature Climate Change*, *10*(7),
963   Article 7. https://doi.org/10.1038/s41558-020-0781-5

964 Lobo, A., Torres-Ruiz, J. M., Burlett, R., Lemaire, C., Parise, C., Francioni, C., Truffaut, L.,
965   Tomášková, I., Hansen, J. K., Kjær, E. D., Kremer, A., & Delzon, S. (2018). Assessing inter-
966   and intraspecific variability of xylem vulnerability to embolism in oaks. *Forest Ecology and*
967   *Management*, *424*, 53–61. https://doi.org/10.1016/j.foreco.2018.04.031

968 Lorenzo-Lacruz, J., Vicente-Serrano, S. M., López-Moreno, J. I., Beguería, S., García-Ruiz, J. M., &
969   Cuadrat, J. M. (2010). The impact of droughts and water management on various
970   hydrological systems in the headwaters of the Tagus River (central Spain). *Journal of*
971   *Hydrology*, *386*(1), 13–26. https://doi.org/10.1016/j.jhydrol.2010.01.001

972 Lu, Y., Sloan, B., Thompson, S. E., Konings, A. G., Bohrer, G., Matheny, A., & Feng, X. (2022). Intra-
973   Specific Variability in Plant Hydraulic Parameters Inferred From Model Inversion of Sap

974 Flux Data. *Journal of Geophysical Research: Biogeosciences*, *127*(6), e2021JG006777.

975 https://doi.org/10.1029/2021JG006777

976 Lübbe, T., Lamarque, L. J., Delzon, S., Torres Ruiz, J. M., Burlett, R., Leuschner, C., & Schuldt, B.

977 (2022). High variation in hydraulic efficiency but not xylem safety between roots and

978 branches in four temperate broad-leaved tree species. *Functional Ecology*, *36*(3), 699–

979 712. https://doi.org/10.1111/1365-2435.13975

980 Mackay, D. S., Roberts, D. E., Ewers, B. E., Sperry, J. S., McDowell, N. G., & Pockman, W. T. (2015).

981 Interdependence of chronic hydraulic dysfunction and canopy processes can improve

982 integrated models of tree response to drought. *Water Resources Research*, *51*(8), 6156–

983 6176. https://doi.org/10.1002/2015WR017244

984 Martínez-Vilalta, J., Prat, E., Oliveras, I., & Piñol, J. (2002). Xylem hydraulic properties of roots and

985 stems of nine Mediterranean woody species. *Oecologia*, *133*(1), 19–29.

986 https://doi.org/10.1007/s00442-002-1009-2

987 Matheny, A. M. (2021). Stressors Reveal Ecosystems' Hidden Characteristics. *Journal of*

988 *Geophysical Research: Biogeosciences*, *126*(8), e2021JG006462.

989 https://doi.org/10.1029/2021JG006462

990 Mauri, A., Girardello, M., Strona, G., Beck, P. S. A., Forzieri, G., Caudullo, G., Manca, F., &

991 Cescatti, A. (2022). EU-Trees4F, a dataset on the future distribution of European tree

992 species. *Scientific Data*, *9*(1), Article 1. https://doi.org/10.1038/s41597-022-01128-5

993 Meinzer, F. C., & McCulloh, K. A. (2013). Xylem recovery from drought-induced embolism: Where

994 is the hydraulic point of no return? *Tree Physiology*, *33*(4), 331–334.

995 https://doi.org/10.1093/treephys/tpt022

996   Mencuccini, M., Manzoni, S., & Christoffersen, B. (2019). Modelling water fluxes in plants: From

997   tissues   to   biosphere.   *New   Phytologist*,   *222*(3),   1207–1222.

998   https://doi.org/10.1111/nph.15681

999   Mirfenderesgi, G., Matheny, A. M., & Bohrer, G. (2019). Hydrodynamic trait coordination and

1000   cost–benefit trade-offs throughout the isohydric–anisohydric continuum in trees.

1001   *Ecohydrology*, *12*(1), e2041. https://doi.org/10.1002/eco.2041

1002   Moreno, A., Neumann, M., & Hasenauer, H. (2017). Forest structures across Europe. *Geoscience*

1003   *Data Journal*, *4*(1), 17–28. https://doi.org/10.1002/gdj3.45

1004   Mrad, A., Domec, J.-C., Huang, C.-W., Lens, F., & Katul, G. (2018). A network model links wood

1005   anatomy to xylem tissue hydraulic behaviour and vulnerability to cavitation. *Plant, Cell &*

1006   *Environment*, *41*(12), 2718–2730. https://doi.org/10.1111/pce.13415

1007   Mrad, A., Sevanto, S., Domec, J.-C., Liu, Y., Nakad, M., & Katul, G. (2019). A Dynamic Optimality

1008   Principle for Water Use Strategies Explains Isohydric to Anisohydric Plant Responses to

1009   Drought.   *Frontiers   in   Forests   and   Global   Change*,   *2*.

1010   https://www.frontiersin.org/articles/10.3389/ffgc.2019.00049

1011   Nelson, J. A., Pérez-Priego, O., Zhou, S., Poyatos, R., Zhang, Y., Blanken, P. D., Gimeno, T. E.,

1012   Wohlfahrt, G., Desai, A. R., Gioli, B., Limousin, J.-M., Bonal, D., Paul-Limoges, E., Scott, R.

1013   L., Varlagin, A., Fuchs, K., Montagnani, L., Wolf, S., Delpierre, N., … Jung, M. (2020).

1014   Ecosystem transpiration and evaporation: Insights from three water flux partitioning

1015   methods   across   FLUXNET   sites.   *Global   Change   Biology*,   *26*(12),   6916–6930.

1016   https://doi.org/10.1111/gcb.15314

1017   Novick, K. A., Konings, A. G., & Gentine, P. (2019). Beyond soil water potential: An expanded view

1018   on isohydricity including land–atmosphere interactions and phenology. *Plant, Cell &*

1019   *Environment*, *42*(6), 1802–1815. https://doi.org/10.1111/pce.13517

1020   Oddi, L., Migliavacca, M., Cremonese, E., Filippa, G., Vacchiano, G., Siniscalco, C., Cella, U. M. di,

1021   & Galvagno, M. (2022). Contrasting responses of forest growth and carbon sequestration

1022   to heat and drought in the Alps. *Environmental Research Letters*, *17*(4), 045015.

1023   https://doi.org/10.1088/1748-9326/ac5b3a

1024   Pappas, C., Fatichi, S., & Burlando, P. (2016). Modeling terrestrial carbon and water dynamics

1025   across climatic gradients: Does plant trait diversity matter? *New Phytologist*, *209*(1), 137–

1026   151. https://doi.org/10.1111/nph.13590

1027   Pelletier, J. D., Broxton, P. D., Hazenberg, P., Zeng, X., Troch, P. A., Niu, G.-Y., Williams, Z., Brunke,

1028   M. A., & Gochis, D. (2016). A gridded global data set of soil, intact regolith, and

1029   sedimentary deposit thicknesses for regional and global land surface modeling. *Journal of*

1030   *Advances   in   Modeling   Earth   Systems*,   *8*(1),   41–65.

1031   https://doi.org/10.1002/2015MS000526

1032   Peñuelas, J., & Filella, I. (2003). Deuterium labelling of roots provides evidence of deep water

1033   access and hydraulic lift by Pinus nigra in a Mediterranean forest of NE Spain.

1034   *Environmental and Experimental Botany*, *49*(3), 201–208. https://doi.org/10.1016/S0098-

1035   8472(02)00070-9

1036   Pereira, L., Domingues-Junior, A. P., Jansen, S., Choat, B., & Mazzafera, P. (2018). Is embolism

1037   resistance in plant xylem associated with quantity and characteristics of lignin? *Trees*,

1038   *32*(2), 349–358. https://doi.org/10.1007/s00468-017-1574-y

1039   Powers, J. S., Vargas G., G., Brodribb, T. J., Schwartz, N. B., Pérez-Aviles, D., Smith-Martin, C. M.,

1040   Becknell, J. M., Aureli, F., Blanco, R., Calderón-Morales, E., Calvo-Alvarado, J. C., Calvo-

1041   Obando, A. J., Chavarría, M. M., Carvajal-Vanegas, D., Jiménez-Rodríguez, C. D., Murillo

1042   Chacon, E., Schaffner, C. M., Werden, L. K., Xu, X., & Medvigy, D. (2020). A catastrophic

1043   tropical drought kills hydraulically vulnerable tree species. *Global Change Biology*, *26*(5),

1044   3122–3133. https://doi.org/10.1111/gcb.15037

1045   Poyatos, R., Granda, V., Flo, V., Adams, M. A., Adorján, B., Aguadé, D., Aidar, M. P. M., Allen, S.,

1046   Alvarado-Barrientos, M. S., Anderson-Teixeira, K. J., Aparecido, L. M., Arain, M. A.,

1047   Aranda, I., Asbjornsen, H., Baxter, R., Beamesderfer, E., Berry, Z. C., Berveiller, D., Blakely,

1048   B., … Martínez-Vilalta, J. (2021). Global transpiration data from sap flow measurements:

1049   The SAPFLUXNET database. *Earth System Science Data*, *13*(6), 2607–2649.

1050   https://doi.org/10.5194/essd-13-2607-2021

1051   Poyatos, R., Granda, V., Flo, V., Molowny-Horas, R., Steppe, K., Mencuccini, M., & Martínez-

1052   Vilalta, J. (2020). *SAPFLUXNET: A global database of sap flow measurements* [Data set].

1053   https://doi.org/10.5281/zenodo.3971689

1054   Reichstein, M., Bahn, M., Mahecha, M. D., Kattge, J., & Baldocchi, D. D. (2014). Linking plant and

1055   ecosystem functional biogeography. *Proceedings of the National Academy of Sciences*,

1056   *111*(38), 13697–13702. https://doi.org/10.1073/pnas.1216065111

1057   Rosner, S., Heinze, B., Savi, T., & Dalla-Salda, G. (2019). Prediction of hydraulic conductivity loss

1058   from relative water loss: New insights into water storage of tree stems and branches.

1059   *Physiologia Plantarum*, *165*(4), 843–854. https://doi.org/10.1111/ppl.12790

1060 Sabot, M. E. B., De Kauwe, M. G., Pitman, A. J., Medlyn, B. E., Verhoef, A., Ukkola, A. M., &

1061   Abramowitz, G. (2020). Plant profit maximization improves predictions of European

1062   forest responses to drought. *New Phytologist*, *226*(6), 1638–1655.

1063   https://doi.org/10.1111/nph.16376

1064 Schirone, B., Vessella, F., & Varela, M. (2019). *EUFORGEN Technical Guidelines for genetic*

1065   *conservation and use for Holm oak (Quercus ilex). European Forest Genetic Resources*

1066   *Programme (EUFORGEN).* European Forest Institute.

1067   http://www.euforgen.org/fileadmin//templates/euforgen.org/upload/Publications/Techn

1068   ical_guidelines/Technical_guidelines_Quercus_ilex.pdf

1069 Schuldt, B., Knutzen, F., Delzon, S., Jansen, S., Müller-Haubold, H., Burlett, R., Clough, Y., &

1070   Leuschner, C. (2016). How adaptable is the hydraulic system of European beech in the

1071   face of climate change-related precipitation reduction? *New Phytologist*, *210*(2), 443–

1072   458. https://doi.org/10.1111/nph.13798

1073 Senf, C., Buras, A., Zang, C. S., Rammig, A., & Seidl, R. (2020). Excess forest mortality is

1074   consistently linked to drought across Europe. *Nature Communications*, *11*(1), 6200.

1075   https://doi.org/10.1038/s41467-020-19924-1

1076 Skelton, R. P., West, A. G., & Dawson, T. E. (2015). Predicting plant vulnerability to drought in

1077   biodiverse regions using functional traits. *Proceedings of the National Academy of*

1078   *Sciences*, *112*(18), 5744–5749. https://doi.org/10.1073/pnas.1503376112

1079 Sloan, B. P., Thompson, S. E., & Feng, X. (2021). Plant hydraulic transport controls transpiration

1080   sensitivity to soil water stress. *Hydrology and Earth System Sciences*, *25*(8), 4259–4274.

1081   https://doi.org/10.5194/hess-25-4259-2021

1082 Song, J., Miller, G. R., Cahill, A. T., Aparecido, L. M. T., & Moore, G. W. (2020). Modeling land

1083   surface processes over a mountainous rainforest in Costa Rica using CLM4.5 and CLM5.

1084   *Geoscientific Model Development*, *13*(11), 5147–5173. https://doi.org/10.5194/gmd-13-

1085   5147-2020

1086 Sperry, J. S., & Love, D. M. (2015). What plant hydraulics can tell us about responses to climate-

1087   change droughts. *New Phytologist*, *207*(1), 14–27. https://doi.org/10.1111/nph.13354

1088 Sturm, J., Santos, M. J., Schmid, B., & Damm, A. (2022). Satellite data reveal differential

1089   responses of Swiss forests to unprecedented 2018 drought. *Global Change Biology*, *28*(9),

1090   2956–2978. https://doi.org/10.1111/gcb.16136

1091 Terradas, J., & Savé, R. (1992). The influence of summer and winter stress and water

1092   relationships on the distribution of Quercus ilex L. *Vegetatio*, *99*(1), 137–145.

1093   https://doi.org/10.1007/BF00118219

1094 Tomasella, M., Nardini, A., Hesse, B. D., Machlet, A., Matyssek, R., & Häberle, K.-H. (2019). Close

1095   to the edge: Effects of repeated severe drought on stem hydraulics and non-structural

1096   carbohydrates in European beech saplings. *Tree Physiology*, *39*(5), 717–728.

1097   https://doi.org/10.1093/treephys/tpy142

1098 UCAR. (2020). *2. CLM Technical Note—Ctsm release-clm5.0 documentation*.

1099   https://escomp.github.io/ctsm-docs/versions/release-clm5.0/html/tech_note/index.html

1100 Venturas, M. D., Sperry, J. S., & Hacke, U. G. (2017). Plant xylem hydraulics: What we understand,

1101   current research, and future challenges. *Journal of Integrative Plant Biology*, *59*(6), 356–

1102   389. https://doi.org/10.1111/jipb.12534

1103   Verheijen, L. M., Brovkin, V., Aerts, R., Bönisch, G., Cornelissen, J. H. C., Kattge, J., Reich, P. B.,

1104   Wright, I. J., & van Bodegom, P. M. (2013). Impacts of trait variation through observed

1105   trait–climate relationships on performance of an Earth system model: A conceptual

1106   analysis. *Biogeosciences*, *10*(8), 5497–5515. https://doi.org/10.5194/bg-10-5497-2013

1107   von Wuehlisch, G. (2008). *EUFORGEN Technical Guidelines for genetic conservation and use for*

1108   *European   beech   (Fagus   sylvatica).*   Bioversity   International.

1109   http://www.euforgen.org/fileadmin//templates/euforgen.org/upload/Publications/Techn

1110   ical_guidelines/Technical_guidelines_Fagus_sylvatica.pdf

1111   Walthert, L., Ganthaler, A., Mayr, S., Saurer, M., Waldner, P., Walser, M., Zweifel, R., & von Arx,

1112   G. (2021). From the comfort zone to crown dieback: Sequence of physiological stress

1113   thresholds in mature European beech trees across progressive drought. *Science of The*

1114   *Total Environment*, *753*, 141792. https://doi.org/10.1016/j.scitotenv.2020.141792

1115   Wang, Y. P., Lu, X. J., Wright, I. J., Dai, Y. J., Rayner, P. J., & Reich, P. B. (2012). Correlations among

1116   leaf traits provide a significant constraint on the estimate of global gross primary

1117   production.   *Geophysical   Research   Letters*,   *39*(19).

1118   https://doi.org/10.1029/2012GL053461

1119   Weithmann, G., Link, R. M., Banzragch, B.-E., Würzberg, L., Leuschner, C., & Schuldt, B. (2022).

1120   Soil water availability and branch age explain variability in xylem safety of European

1121   beech in Central Europe. *Oecologia*, *198*(3), 629–644. https://doi.org/10.1007/s00442-

1122   022-05124-9

1123   Willigen, C. V., Sherwin, H. W., & Pammenter, N. W. (2000). Xylem hydraulic characteristics of

1124   subtropical trees from contrasting habitats grown under identical environmental

1125   conditions. *The New Phytologist*, *145*(1), 51–59. https://doi.org/10.1046/j.1469-

1126   8137.2000.00549.x

1127 Xu, X., Medvigy, D., Powers, J. S., Becknell, J. M., & Guan, K. (2016). Diversity in plant hydraulic

1128   traits explains seasonal and inter-annual variations of vegetation dynamics in seasonally

1129   dry tropical forests. *New Phytologist*, *212*(1), 80–95. https://doi.org/10.1111/nph.14009

1130 Zapater, M., Hossann, C., Bréda, N., Bréchet, C., Bonal, D., & Granier, A. (2011). Evidence of

1131   hydraulic lift in a young beech and oak mixed forest using 18O soil water labelling. *Trees*,

1132   *25*(5), 885. https://doi.org/10.1007/s00468-011-0563-9

1133
1134

1135 **Table 1.** Summary of the environmental characteristics of each experimental site. All data is
1136 based on Poyatos et al. (2021) except those explicitly mentioning the source.

	DE-Hin	ES-Alt	FR-Hes	FR-Pue
Country	Germany	Spain	France	France
Site Name	Hinnensee	Alto Tajo	Hesse	Puechabon
Latitude (°)	53.33	40.802	48.674	43.741
Longitude (°)	13.192	-2.230	7.065	3.596
Elevation (m a.s.l.)	90	981	300	270
Mean Annual Precipitation (mm yr^{-1})	606.40	566.90	1003.48	1022.97
Mean Annual Temperature (°C)	8.68	11.74	9.97	13.80
Köppen-Geiger Climate Classification (Beck et al., 2018)	Cfb	Csb	Cfb	Csa
Slope (%)	2-5	5-10	0-2	0-2
Soil Texture	Sandy	n.a.	Silty	Clay-Loam
Soil Depth (cm)	n.a.	n.a.	120	52.5
Species under analysis	*Fagus sylvatica*	*Quercus ilex*	*Fagus sylvatica*	*Quercus ilex*
Stand Age (yr)	~200	59	34	58
Stand Basal Area (m^2 ha^{-1})	n.a.	13.1	19.7	28.1
Stand Height (m)	24.0	4.9	13.0	5.0
Period of Analysis	2012-2014	2012-2014	2001-2005	2001-2005

1137
1138

1139 **Table 2.** Plant hydraulic traits describing the vulnerable and resistant curves of the two selected
1140 tree species.

	Parameter	Units	*Fagus sylvatica*	*Quercus ilex*
Default Model Configuration	k_{max}	mm$_{H2O}$ mm$_{H2O}$$^{-1}$s^{-1}	2 x 10^{-8}	2 x 10^{-8}
	c_k	-	3.95	3.95
	Ψ_{p50}	MPa	-2.70	-2.70
Vulnerable Tree Configuration	k_{max}	mm$_{H2O}$ mm$_{H2O}$$^{-1}$s^{-1}	2 x 10^{-8}	2 x 10^{-8}
	c_k	-	1.73	1.70
	Ψ_{p50}	MPa	-1.90	-1.23
Resistant Tree Configuration	k_{max}	mm$_{H2O}$ mm$_{H2O}$$^{-1}$s^{-1}	2 x 10^{-8}	2 x 10^{-8}
	c_k	-	3.33	8.04
	Ψ_{p50}	MPa	-4.7	-5.72

1141
1142